Old groundwater in parts of the upper Patapsco aquifer, Atlantic Coastal Plain, Maryland, USA: evidence from radiocarbon, chlorine-36 and helium-4

L. N. Plummer, J. R. Eggleston, D. C. Andreasen, J. P. Raffensperger, A. G. Hunt & G. C. Casile

Hydrogeology Journal
Official Journal of the International Association of Hydrogeologists

ISSN 1431-2174

Hydrogeol J
DOI 10.1007/s10040-012-0871-1

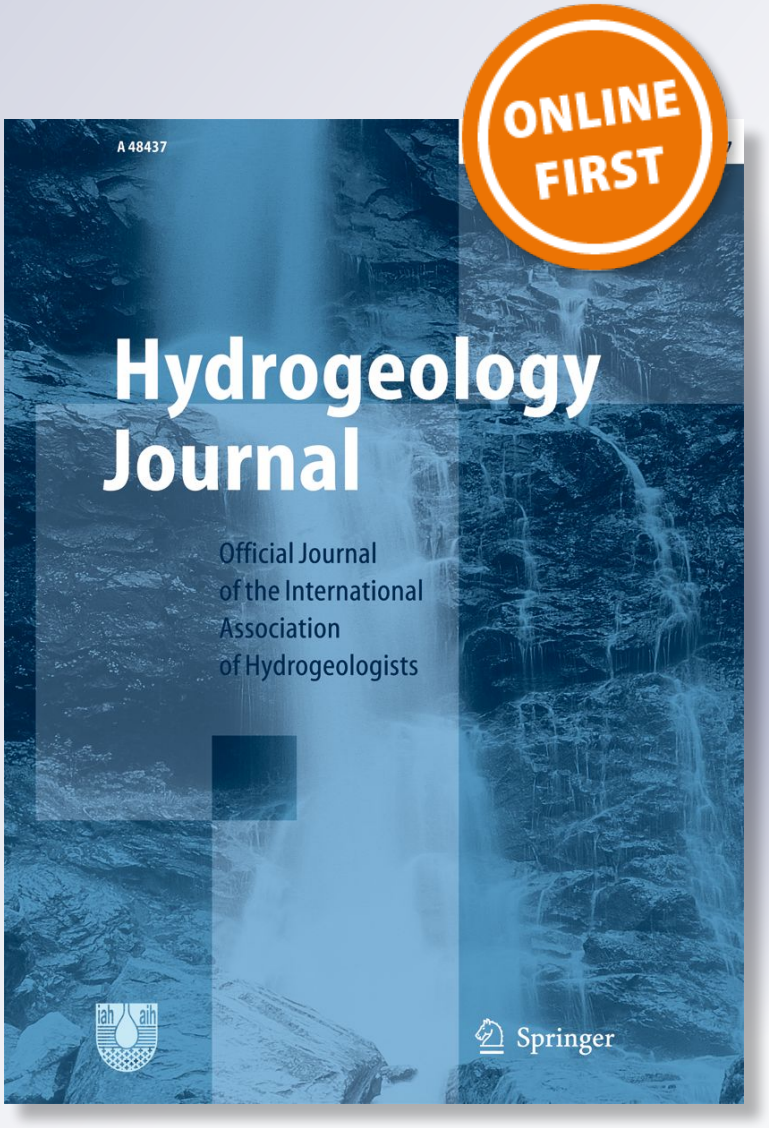

Springer

Old groundwater in parts of the upper Patapsco aquifer, Atlantic Coastal Plain, Maryland, USA: evidence from radiocarbon, chlorine-36 and helium-4

L. N. Plummer · J. R. Eggleston · D. C. Andreasen · J. P. Raffensperger · A. G. Hunt · G. C. Casile

Abstract Apparent groundwater ages along two flow paths in the upper Patapsco aquifer of the Maryland Atlantic Coastal Plain, USA, were estimated using ^{14}C, ^{36}Cl and ^{4}He data. Most of the ages range from modern to about 500ka, with one sample at 117km downgradient from the recharge area dated by radiogenic ^{4}He accumulation at more than one Ma. Last glacial maximum (LGM) water was located about 20km downgradient on the northern flow path, where the radiocarbon age was 21.5ka, paleorecharge temperatures were 0.5–1.5 °C (a maximum cooling of about 12 °C relative to the modern mean annual temperature of 13 °C), and Cl^-, Cl/Br, and stable isotopes of water were minimum. Low recharge temperatures (typically 5–7 °C) indicate that recharge occurred predominantly during glacial periods when coastal heads were lowest due to low sea-level stand. Flow velocities averaged about 1.0 m a^{-1} in upgradient parts of the upper Patapsco aquifer and decreased from 0.13 to 0.04 m a^{-1} at 40 and 80km further downgradient, respectively. This study demonstrates that most water in the upper Patapsco aquifer is non-renewable on human timescales under natural gradients, thus highlighting the importance of effective water-supply management to prolong the resource.

Keywords Coastal aquifers · Groundwater age · Radioactive isotopes · Atlantic Coastal Plain · USA

Received: 5 August 2011 / Accepted: 4 May 2012

Electronic supplementary material The online version of this article (doi:10.1007/s10040-012-0871-1) contains supplementary material, which is available to authorized users.

L. N. Plummer (✉) · G. C. Casile
US Geological Survey,
432 National Center, Reston, VA 20192, USA
e-mail: nplummer@usgs.gov
Tel.: +1-703-648-5841
Fax: +1-703-648-5832

J. R. Eggleston
US Geological Survey,
79 Greenough St., Brookline, MA 02445, USA

D. C. Andreasen
Maryland Geological Survey,
2300 St. Paul Street, Baltimore, MD 21218, USA

J. P. Raffensperger
US Geological Survey,
5522 Research Park Drive, Baltimore, MD 21228, USA

A. G. Hunt
US Geological Survey, Denver Federal Center,
BLD 21, MS 963, Denver, CO 80225, USA

Introduction

Estimates of groundwater age, as interpreted from measurements of concentrations of naturally occurring environmental tracers, can be used to identify those parts of aquifers that may be non-renewable on human timescales (Gleeson et al. 2010). In this study, groundwater age was interpreted from measurements of the concentrations of a suite of environmental tracers in parts of the upper Patapsco aquifer of the Atlantic Coastal Plain of Maryland, USA, which increasingly is being utilized for freshwater supply, but for which there have been no previous measurements to estimate groundwater age.

Groundwater withdrawals have contributed to declines in water levels of as much as 30 m since the pre-1960 levels in parts of the Maryland Coastal Plain (Drummond 2007; Soeder et al. 2007), altering groundwater flow patterns in most areas of the Coastal Plain aquifer system. Water levels in many of the confined aquifers of Southern Maryland and parts of the Eastern Shore (east of Chesapeake Bay) currently are declining at a rate of about 0.6 m a^{-1} (Shedlock et al. 2007) in areas where the population is expected to grow significantly in the next 20–30 years. Concerns over saltwater intrusion and arsenic contamination have led water managers to increasingly move groundwater production from the Aquia aquifer to the underlying upper Patapsco aquifer, which has caused groundwater levels to decline (Drummond 2007). Future management of the groundwater resources of the Atlantic Coastal Plain of Maryland, and elsewhere

DOI 10.1007/s10040-012-0871-1

Published online: 07 June 2012

along the Mid-Atlantic Coastal Plain of the US is critical to meeting the long term needs of this region.

The tracer measurements of this study, and the approximate timescales they potentially represent are as follows: (1) tritium (^{3}H), tritium/helium-3 ($^{3}H/^{3}He$), chlorofluorocarbons (CFCs, CFC-12, CFC-11, CFC-113), and sulfur hexafluoride (SF_6), (post-1950 timescale, or mixtures of older water containing fractions of post-1950 water), (2) carbon-14 (^{14}C) of dissolved inorganic carbon (approximately 1–30 ka age range, or mixtures of older and younger water), (3) chlorine-36 (^{36}Cl) of dissolved chloride (potentially 50 ka to approximately 1×10^{6} year timescale, or mixtures), and (4) dissolved helium-4 (^{4}He), (approximately 100 years to potentially more than 1×10^{6} year timescale, or possible mixtures). Measurements of noble gases (helium (He), argon (Ar), neon (Ne), xenon (Xe), and krypton (Kr)), dissolved major gases (N_2, Ar, CO_2, CH_4), stable isotopes of water (^{2}H, ^{18}O), and inorganic water chemistry are included because they can help to recognize paleoclimatic signals in groundwater and, in some cases, help corroborate interpreted groundwater ages. Taken together, measurements of the concentrations of this suite of environmental tracers can potentially identify waters recharged on a timescale from modern to more than 1 million years. Other temporal information can be interpreted from the Cl^- concentration, the Cl/Br ratio and the $^{36}Cl/Cl$ ratio which are functions of distance of the recharge zone from the Atlantic Ocean, due to the rise and fall of sea level through previous glacial cycles, and thus provide additional means of testing validity of interpreted groundwater ages (Phillips 2000; Aeschbach-Hertig et al. 2002; Purdy et al. 1996).

Hydrogeologic setting

The Atlantic Coastal Plain of Maryland consists of a series of wedge-shaped sedimentary units that thicken in an east–southeast direction from the fall line or line of contact with the consolidated, crystalline rocks of the Piedmont Province. The fall line strikes approximately northeast passing through Washington, DC and the city of Baltimore, MD (Fig. 1). The Coastal Plain sediments consist of interstratified layers of unconsolidated, sand, gravel, silt, and clay of varying extent and thickness. During geologic time, changes in sea level created alternating non-marine (fluvial-deltaic), fluvio-marine, and marine sedimentary environments. The resulting sediments range in age from early Cretaceous to Holocene and deepen to the east–southeast with a slope of approximately 5–12 m km^{-1} (Andreasen et al. 2007; Drummond 2007) within a structural depression known as the Salisbury Embayment (Richards 1948). Thickness of the Coastal Plain sediments increases from a feather edge near the fall line to as much as 900 m along the western margin of Chesapeake Bay, and more than 2,300 m at the Atlantic Ocean coastline (Andreasen et al. 2007).

At least seven major aquifers are recognized in the Atlantic Coastal Plain of Maryland, all of which are a part of the larger Northern-Atlantic Coastal Plain aquifer system (Masterson et al. 2011). From shallow to deep, these aquifers in Maryland are the Surficial, Piney Point, Aquia, Magothy, upper Patapsco, lower Patapsco, and Patuxent (Fig. 2). All are used for water supply to varying extents in various parts of the Maryland Atlantic Coastal Plain. Geologic mapping and groundwater models (Andreasen 2007; Drummond 2007) show that the upper Patapsco aquifer is recharged along a narrow outcrop belt that is less than 8 km wide, extending approximately 225 km parallel to the fall line at a position about 10 km to the southeast of the fall line (Fig. 1).

Under pre-pumping conditions, the upper Patapsco aquifer was recharged by infiltration of precipitation within the outcrop belt that flowed southeast along parts of the southern (S–S') and northern transects (N–N') (Fig. 1). Prior to development in the late 1800s, groundwater in the deep confined aquifers such as the upper Patapsco aquifer discharged to overlying layers and ultimately to the Atlantic Ocean, Chesapeake Bay, or tidal estuaries and surface water. During periods of high sea-level stand such as in the modern era, most upper Patapsco groundwater would likely discharge to tidal surface waters on the west side of the Chesapeake Bay, because those water bodies provide the steepest downgradient path to sea level (Fig. 3). However, in earlier eras, discharge areas and groundwater flow directions within the upper Patapsco aquifer likely responded to changes in sea level. Over the past 1 million years, sea level has fluctuated from about 10 m higher to about 125 m lower than present-day sea level (Bintanja et al. 2005). At low sea-level stands, the Chesapeake Bay would likely be absent in Maryland and the ultimate discharge area for upper Patapsco groundwater may have been further east, along the shore of the Atlantic Ocean (Fig. 3).

Under modern-day pumping rates, flow directions and flow rates have changed dramatically from those of pre-pumping conditions (Drummond 2007). In 2002, more than 10 times as much water was pumped from the upper Patapsco in the Maryland Atlantic Coastal Plain than was recharged to the aquifer under pre-pumping conditions. Most groundwater discharging to tidal areas during pre-pumping times is captured by pumping wells under 2002 pumping conditions (Drummond 2007).

The wells sampled in this investigation are screened in the upper Patapsco aquifer along two transects (N–N' and S–S') that are roughly aligned downdip through the central and southern portions of the Maryland Coastal Plain and assumed to parallel paleo groundwater flow paths (Figs. 1, 3, and 4). The well screens are mostly positioned in the upper to middle portions of the aquifer. The upper Patapsco aquifer consists of a sequence of 50–180 m of interbedded fine- to medium-grained quartzose sands, and variegated (gray, brown, red) silt and clay of the upper portion of the fluvial-deltaic Patapsco Formation. The aquifer is regionally extensive within the Maryland Coastal Plain and extends southwest beneath the Potomac

 DOI 10.1007/s10040-012-0871-1

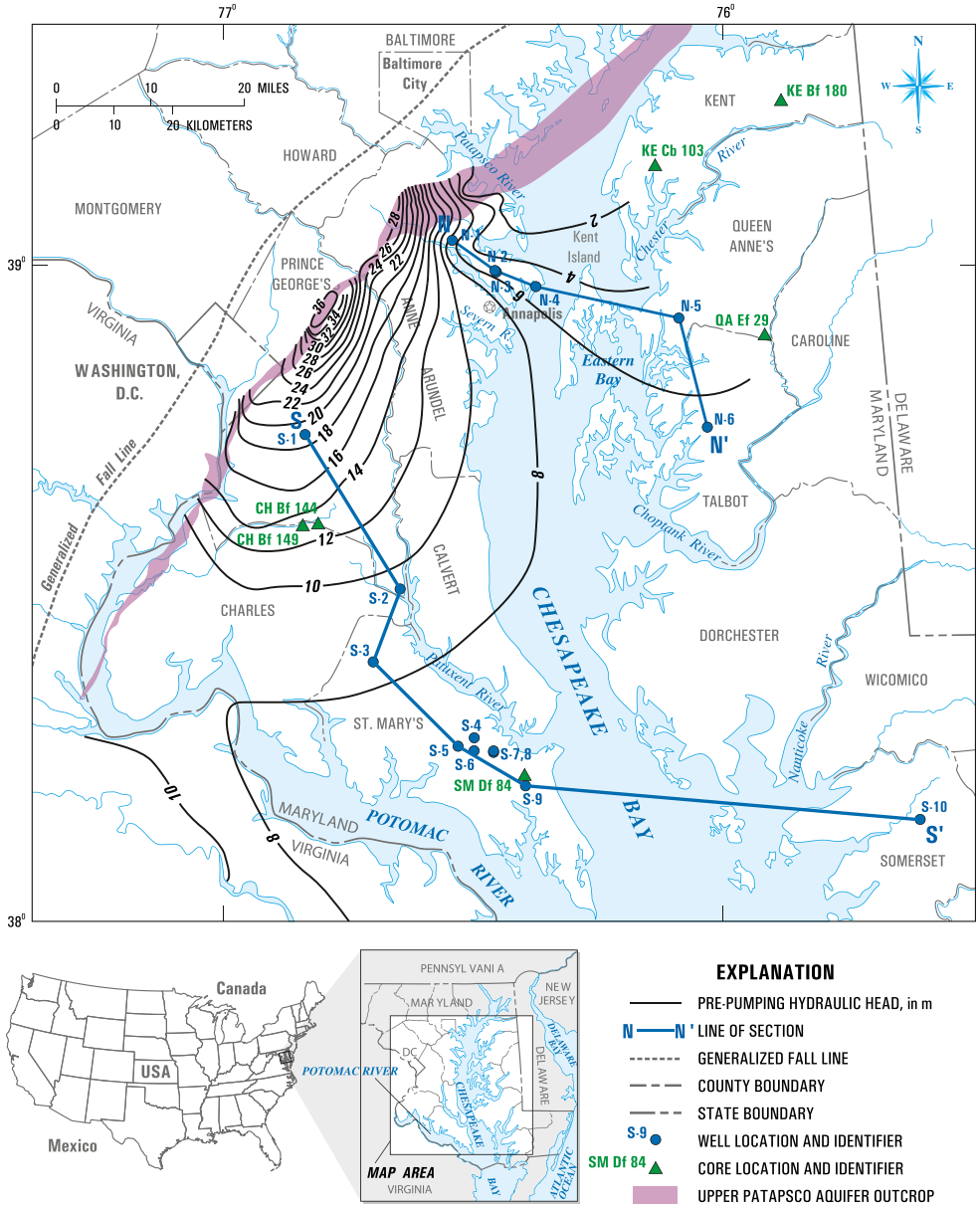

Fig. 1 Map showing study area, water well and core sample locations, outcrop area of the upper Patapsco aquifer, locations of cross sections shown in Fig. 4, the modern, pre-pumping hydraulic heads, and relation to Chesapeake Bay and the fall line. The transects N–N′ and S–S′ are positioned along generalized flow directions that likely have varied in the past (see Fig. 3) and do not necessarily conform to the modern pre-development potentiometric surface

River into Virginia; the Potomac Group aquifers in Virginia, however, are undifferentiated (McFarland and Bruce 2006). Clay-rich units in the top of the Patapsco Formation and bottom of the Magothy Formation, named the Magothy-Patapsco confining unit, separate the upper Patapsco aquifer from the overlying Magothy aquifer (Andreasen et al. 2007). Where the Magothy Formation is truncated, the upper Patapsco aquifer is overlain by the Aquia aquifer and separated from the Aquia by clays predominantly of the Patapsco Formation (Andreasen et al. 2007). The upper Patapsco aquifer is separated from the lower Patapsco aquifer by the Patapsco confining unit (Andreasen et al. 2007).

The main axis of the river system that deposited the fluvial-deltaic Patapsco Formation trended southeast through Baltimore City and northern Anne Arundel County (Hansen 1969). Sand percentages and aquifer transmissivity diminish significantly from north to south between the two depositional environments (Hansen 1969). The northern transect (N–N') is characterized by massive sands that appear blocky on resistivity logs and are relatively continuous between boreholes (Fig. 4a), while sands along the southern transect (S–S') are thinner and less easily correlated between boreholes (Fig. 4b). This difference in deposition results in hydraulic connections (pathways) within the upper Patapsco aquifer that

 DOI 10.1007/s10040-012-0871-1

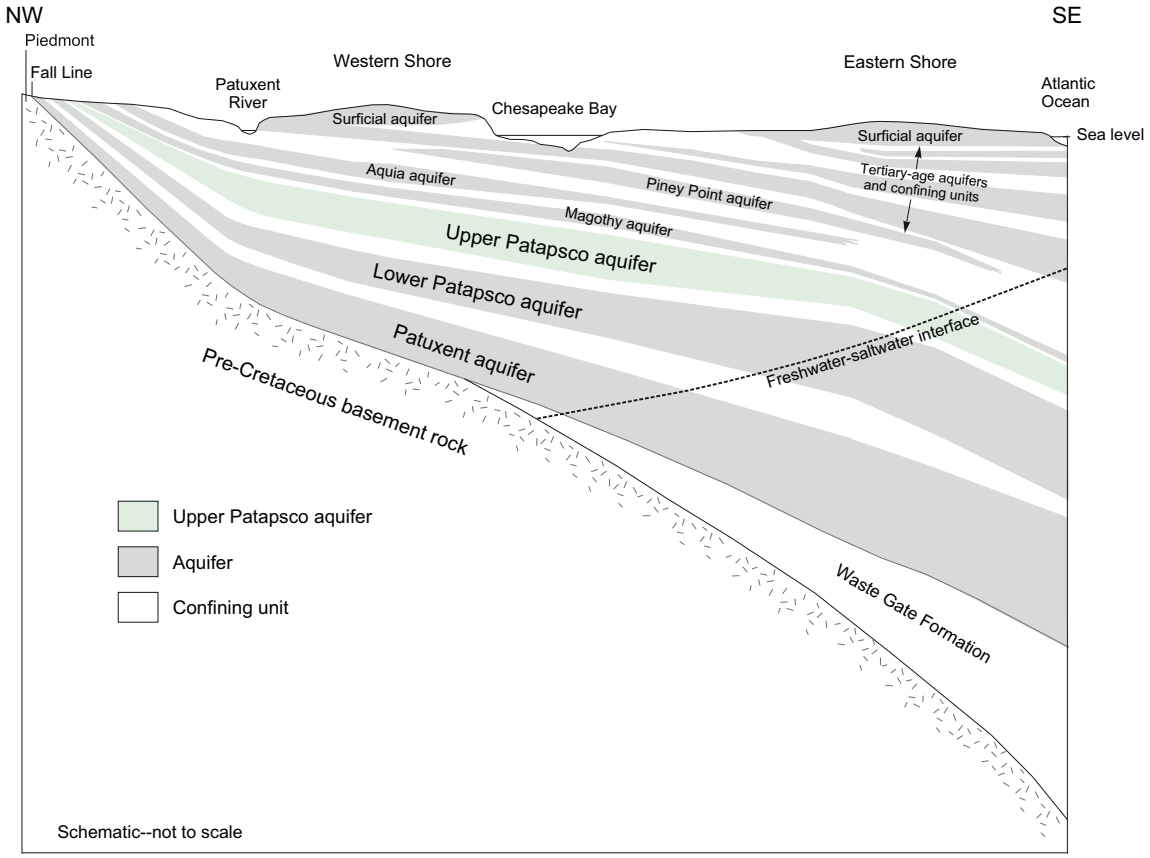

Fig. 2 Generalized cross section showing major aquifers and confining units in the sedimentary wedge of the Maryland Atlantic Coastal Plain

may be more direct along the northern transect and more tortuous along the southern transect. As a consequence, groundwater flow paths may be longer in the upper Patapsco aquifer in the southern portion of the Maryland Coastal Plain, than the northern part.

The Magothy-Patapsco confining unit separating the upper Patapsco and Magothy aquifers is relatively thick (20 m) in the downdip portion of the northern transect (Fig. 4a). The confining unit thins to a few meters in the updip portion where the upper sand of the upper Patapsco aquifer likely is hydraulically connected to the Magothy aquifer. Correlation of water levels in the Magothy aquifer with withdrawals from the upper Patapsco aquifer supports a hydraulic connection between the Magothy aquifer and upper Patapsco aquifer in the updip region (Fleck and Andreasen 1996).

Groundwater travel distances along the northern and southern transects were calculated by projecting sampling points onto two flow paths trending to the southeast from the fall line during periods of low sea-level stand (Fig. 3). The estimated flow distances are given in Table 1 and in the electronic supplemental material (Table ESM1). The flow history of groundwater has greater uncertainty at sample point S-10 where groundwater flow directions may have reversed over time to and from the Chesapeake Bay and Atlantic Ocean. Travel time is therefore not related to travel distance at the S-10 location as it is at the other sample points. Without a detailed understanding or numerical simulation of paleo-flow regimes under various sea-level stands, the historic groundwater flow paths and flow distances near sample S-10 are uncertain.

Sample collection, and analytical procedures

Water samples from 16 wells in the upper Patapsco aquifer of Maryland were collected in March 2010 on the northern and southern transects (Fig. 1). Seven of the original 16 wells were re-sampled to include chlorine-36 in September 2010. All the sampled wells were public supply or production wells with existing submersible or vertical turbine pumps. An inventory of candidate wells in the upper Patapsco was compiled; the list was further reduced to those open only to the upper Patapsco and those located near the anticipated hypothetical northern and southern flow paths. After inspection in the field, some of these wells were not suitable for sampling. Though closely spaced, a cluster of wells (S-4 through S-8) showed that the chemistry and isotopic composition of groundwater in the upper Patapsco could be repeated in samples from nearby wells. Well depths ranged from 56 to 378 m below land surface (bls) and the total interval of upper Patapsco aquifer intercepted by the well screen(s) ranged from 5 to 65 m (Fig. 4).

 DOI 10.1007/s10040-012-0871-1

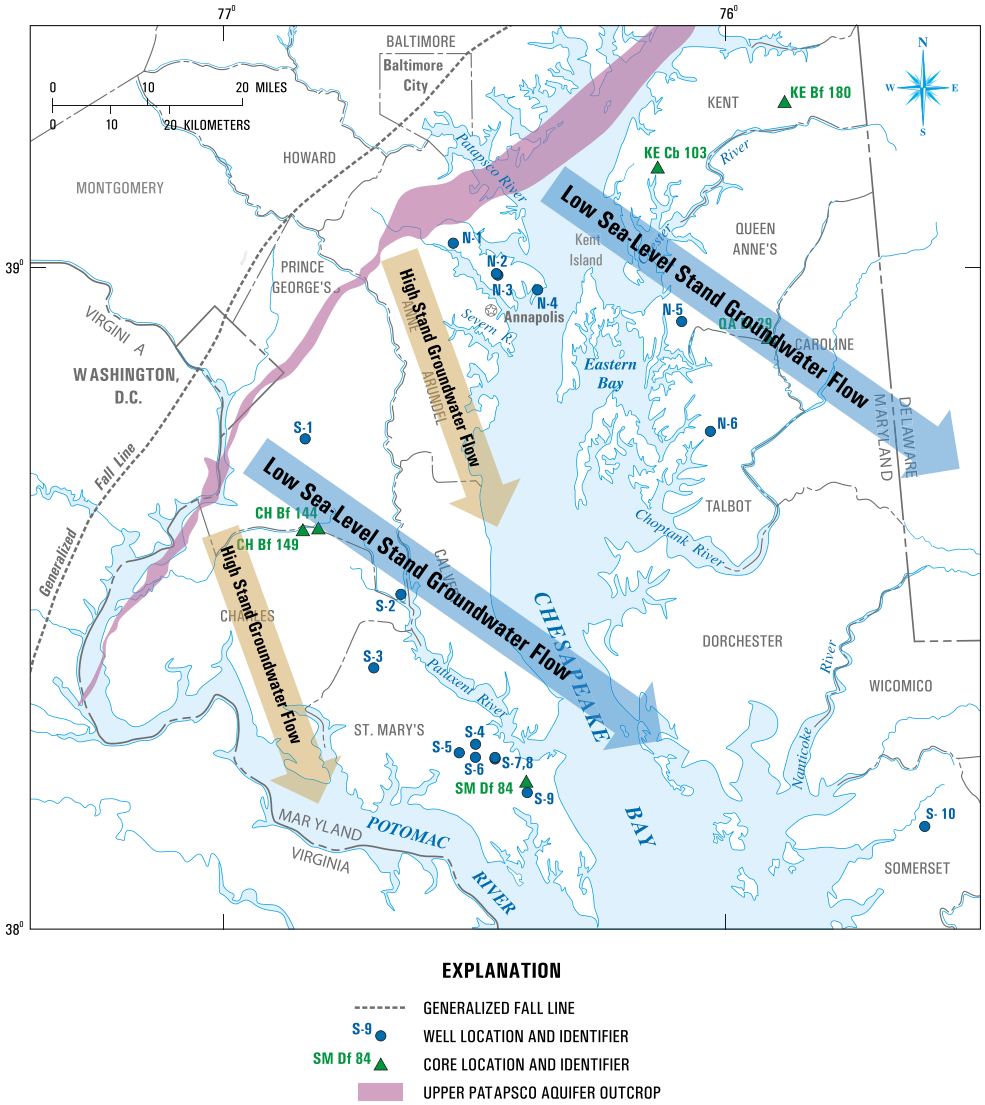

Fig. 3 Map showing conceptualization of generalized groundwater flow directions in the upper Patapsco during periods of high sea-level stand (interglacial periods such as today), and during periods of low sea-level stand (glacial periods)

Replicate quality assurance/quality control (QA/QC) samples were collected at two of the wells (N-5 and S-6), for a total of 18 samples in the March 2010 sampling. Field procedures generally follow those given in Koterba et al. (1995) and the USGS National Field Manual (US Geological Survey variously dated), except as given in the following. Dissolved oxygen concentrations, which typically were below detection using a multi-meter, were measured using a portable field spectrophotometer by the indigo carmine method.

The ^{14}C samples were filtered through disposable filters with 0.45 micron pore size and collected in 1-L glass bottles with polyseal cone cap. They were sealed with an approximately 1 cc air headspace. The samples for CFCs, stable isotopes of water, tritium, SF_6, noble gases, and dissolved major gases were raw, unfiltered water. Collection procedures for stable isotopes are given at US Geological Survey (2011a), and for CFCs, SF_6 and dissolved gases at US Geological Survey (2011b).

Noble gas samples were crimped in re-sealable copper tubes using a back-pressure system to decrease the possibility of bubble formation and degassing of the sample water during collection. This apparatus allows sample water to flow through two loops, a by-pass loop and a loop containing the copper sample tube. Noble gases were measured at the USGS Noble Gas Laboratory, Lakewood, Colorado, by methods similar to those of Bayer et al. (1989) and Beyerle et al. (2000). One-sigma uncertainties for mass spectrometric determination of noble gases are: ^{4}He, 1 %, Ne and Ar, 2 %, Kr, and Xe, 3 %.

The noble gas and dissolved permanent gas concentrations were used to calculate recharge temperature and quantities of excess air. The recharge temperature is the temperature at the water table in the recharge zone at the time of separation from the atmosphere during recharge. In shallow recharge zones such as the eastern Mid-Atlantic Coastal Plain, the recharge temperature corresponds closely

 DOI 10.1007/s10040-012-0871-1

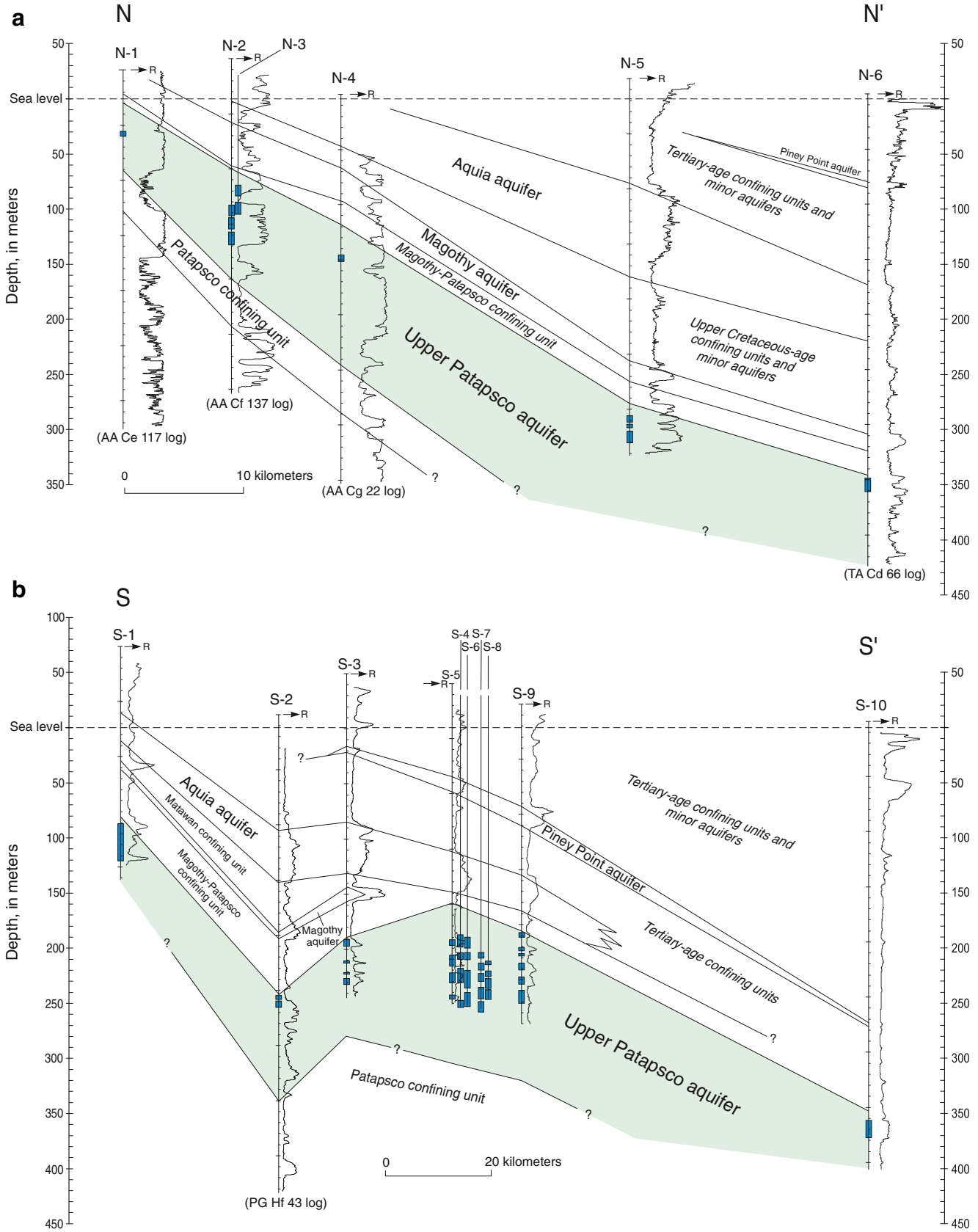

Fig. 4 Cross sections along the **a** northern and **b** southern flow paths (Fig. 1) showing locations of wells sampled, intervals open to the upper Patapsco, resistivity logs (*R*), and location of adjacent aquifers and confining layers

 DOI 10.1007/s10040-012-0871-1

Table 1 Summary of chemical analyses of water from the upper Patapsco aquifer. *ND* not determined

Site no.	Well name	Date	Flow distance, km	Temp °C	DO[a] mg L^{-1}	pH	K_{25} µS cm^{-1}	Ca^{2+} mg L^{-1}	Mg^{2+} mg L^{-1}	Na^{+} mg L^{-1}	K^{+} mg L^{-1}	Fe^{2+} mg L^{-1}	Mn^{2+} mg L^{-1}	HCO_3^{-} mg L^{-1}	Cl^{-} mg L^{-1}	SO_4^{2-} mg L^{-1}	NO_3^{-} as N mg L^{-1}	F^{-} mg L^{-1}	Br^{-} mg L^{-1}	Cl/Br wt. ratio	As µg L^{-1}
N-1	AA Ce 96	3/8/2010	5.3	13.0	5.4	4.33	108	2.63	1.80	8.20	1.1	0.10	0.014	<2	17.7	8.13	2.53	<0.05	0.056	316	<0.1
N-2	AA Cf 119	3/8/2010	14.2	15.5	0.15	4.84	99	3.64	2.07	1.01	1.4	10.9	0.185	<2	1.10	57.8	<0.02	0.23	0.011	103	0.6
N-3	AA Cf 155	3/8/2010	14.6	15.4	ND	5.51	105	4.30	2.51	1.02	1.5	13.2	0.228	14.4	0.88	58.9	0.02	0.43	0.010	87	0.8
N-4	AA Cg 19	3/12/2010	21.7	15.5	0.14	6.04	153	5.18	2.90	1.10	1.7	25.2	0.369	40.2	0.66	56.3	0.02	0.10	0.007	90	1.0
N-4[b]	AA Cg 19	9/28/2010	21.7	17.8	ND	6.20	167	5.43	2.93	1.20	1.8	27.2	0.390	44.2	0.53	38.4	<0.02	0.08	0.009	58	1.1
N-5	QA Ed 45	3/9/2010	45.3	19.3	0.08	6.72	149	10.9	5.19	4.94	5.0	5.91	0.105	65.7	1.29	22.1	0.02	0.16	0.009	143	0.2
N-5[c]	QA Ed 45	3/9/2010	45.3	19.3	0.08	6.72	149	10.4	4.92	4.43	4.7	5.74	0.103	65.1	1.32	21.7	0.02	0.16	0.009	151	0.2
N-5[b]	QA Ed 45	9/28/2010	45.3	20.9	ND	6.65	159	11.0	4.87	4.89	4.9	5.33	0.099	62.4	1.21	19.9	<0.02	0.19	0.009	140	0.2
N-6	TA Ce 70	3/9/2010	59.1	24.7	0.05	7.35	161	2.76	1.82	24.9	6.1	0.84	0.027	78.9	1.56	14.2	<0.02	0.19	0.013	122	<0.1
N-6[b]	TA Ce 70	9/28/2010	59.1	26.1	ND	7.04	170	2.82	1.77	26.6	6.1	0.90	0.021	76.3	1.49	14.6	<0.02	0.22	0.012	123	0.1
S-1	PG Ed 60	3/10/2010	10.8	15.2	0.09	7.56	244	40.1	6.20	2.90	3.0	0.75	0.016	146.6	1.20	7.48	<0.02	0.17	0.013	94	<0.1
S-2	PG Hf 49	3/12/2010	41.4	20.3	0.12	7.21	268	17.0	11.5	15.6	9.0	1.19	0.012	164.8	0.89	4.87	<0.02	0.37	0.009	104	<0.1
S-2[b]	PG Hf 49	9/29/2010	41.4	20.8	ND	7.12	265	17.5	12.3	16.1	9.3	1.19	0.014	165.2	0.81	4.53	<0.02	0.37	0.008	101	0.2
S-3	SM Bc 41	3/10/2010	50.3	19.6	0.08	8.19	237	0.55	0.38	52.3	3.5	0.31	0.011	145.1	1.12	6.86	<0.02	0.35	0.010	111	<0.1
S-4	SM De 59	3/10/2010	69.7	19.6	0.08	8.29	233	0.25	0.23	51.2	3.0	0.08	0.009	148.4	1.79	3.64	<0.02	0.26	0.016	113	0.1
S-4[c]	SM De 59	3/10/2010	69.7	19.6	0.08	8.29	233	0.27	0.23	54.2	3.1	0.08	0.009	148.7	1.79	3.69	<0.02	0.24	0.015	117	0.1
S-4[b]	SM De 59	9/29/2010	69.7	20.1	ND	8.02	235	0.27	0.24	54.0	3.1	0.11	0.008	145.1	1.64	3.52	<0.02	0.27	0.013	125	0.2
S-5	SM Dd 78	3/11/2010	69.7	19.6	0.05	8.32	234	0.23	0.18	53.1	2.4	0.09	0.006	148.8	1.77	3.37	<0.02	0.24	0.015	121	0.2
S-6	SM De 60	3/11/2010	71.7	19.7	0.05	8.44	244	0.19	0.18	56.6	2.7	0.04	0.007	156.0	1.70	3.20	<0.02	0.27	0.014	119	<0.1
S-7	SM De 52	3/11/2010	73.3	19.8	0.04	8.47	260	0.38	0.32	67.7	2.7	0.05	0.009	177.6	1.56	5.84	<0.02	0.35	0.013	117	<0.1
S-8	SM De 51	3/11/2010	73.5	20.3	0.05	8.42	270	0.29	0.26	62.5	2.5	0.04	0.007	170.7	1.57	6.11	<0.02	0.32	0.013	123	<0.1
S-9	SM Ef 94	3/11/2010	81.0	20.4	0.16	8.39	265	0.44	0.30	61.1	2.7	0.04	0.011	168.3	1.56	5.49	<0.02	0.35	0.013	117	<0.1
S-9[b]	SM Ef 94	9/29/2010	81.0	20.7	ND	8.14	268	0.47	0.30	63.8	3.0	0.04	0.011	164.5	1.48	5.30	<0.02	0.40	0.012	119	0.1
S-10	SO Be 116	3/9/2010	117.3	27.8	0.09	8.59	1382	1.31	0.89	351	6.9	0.03	0.007	806.0	65.3	40.5	<0.02	3.70	0.282	232	0.3
S-10[b]	SO Be 116	10/4/2010	117.3	27.2	ND	8.34	1418	1.39	0.89	362	7.0	0.03	0.007	802.7	64.3	40.3	<0.02	3.88	0.260	247	0.3

[a] DO by Indigo Carmine Method, except for sample AA Ce 96 which was measured using field multi-parameter meter

[b] Re-sampled for ^{36}Cl analysis

[c] Replicate analysis, QA/QC

DOI 10.1007/s10040-012-0871-1

to the mean annual temperature at the water table (Stute and Schlosser (2000). The modern mean-annual temperature of shallow groundwater in the study area is approximately 13 °C. Excess air is the quantity of air trapped during recharge and dissolved in groundwater (Aeschbach-Hertig et al. 1999; Aeschbach-Hertig et al. 2000). Two models were considered in calculating the recharge temperature and excess-air component: (1) the unfractionated excess-air model (UA model) which was applied to the N_2–Ar data, and (2) the closed-system equilibration (CE) model which was applied to the noble gas (Ar, Ne, Xe, Kr) data (Aeschbach-Hertig et al. 1999, 2000). Monte Carlo simulation using 3,000 synthetic samples based on the errors of the measured gases was performed to generate the range of one standard deviation (1σ) uncertainties for the model parameters– the noble-gas recharge temperature (NGRT), the initial amount of entrapped air (A_e), the reduction of volume of entrapped air due to dissolution (F), and the sum of the weighted squared deviations between modeled and measured noble-gas concentrations (χ^2) (Aeschbach-Hertig et al. 1999; Aeschbach-Hertig et al. 2000). In cases of poor model fit, the evaluation of data fit to the model removed suspect gases (Kr data typically) to produce the recharge model parameters. In some cases this parameter manipulation forced the model to only account for unfractionated excess air (UA model) due to parameter constraints.

Other methods of analysis are generally those described in Plummer et al. (2004). Inorganic water chemistry was determined by Inductively Coupled Plasma Mass Spectrometry (ICPMS) and ion chromatography (IC) in the USGS National Research Program Water-Chemistry Laboratory, Reston, Virginia (VA). An ICPMS analytical procedure (Davis et al. 2004) was used to determine Br^- concentrations that typically were ten-fold below the IC detection limit of 0.05 mg L^{-1}. The radiocarbon samples were acidified and collected as CO_2 gas, converted to graphite and measured by accelerator mass spectrometry (AMS) at the National Ocean Sciences Accelerator Mass Spectrometry Facility (NOSAMS; Woods Hole Oceanographic 2011), Woods Hole, MA. Major dissolved gases (N_2, Ar, CO_2, O_2, and CH_4) and ^{4}He were measured by gas chromatography at the USGS Dissolved Gas Laboratory, Reston, VA (US Geological Survey 2011c). Analytical uncertainties typically are <1 % for N_2, and Ar, and 1–2 % for CO_2 and CH_4. Calculated equilibration temperatures for analyzed air-equilibrated water standards prepared at 9.0, 16.0 and 24.0 °C typically were within±0.3 °C of the actual water temperature using the GC N_2–Ar data. An overall uncertainty of ±0.5 °C was assigned to the GC N_2–Ar recharge temperatures because, although nitrate concentrations would be negligibly low in paleorecharge in the Mid-Atlantic region, denitrification was not considered in calculation of paleorecharge temperatures. There is no evidence of excess N_2 in the dissolved gas analyses of the paleowaters.

CFCs and SF_6 were determined by purge and trap gas chromatography with electron capture detector at the USGS Reston Chlorofluorocarbon Laboratory, Reston VA (US Geological Survey 2011b), using methods similar to those of Busenberg and Plummer (1992). Minimum detection limits for CFCs were 0.01 pmol kg^{-1} for CFCs and 0.05 femtomoles (fmol) kg^{-1} for SF_6. Tritium was determined at the USGS Low-level Tritium Laboratory, Menlo Park, CA by electrolytic enrichment and liquid scintillation counting, with 1σ uncertainties typically of ±0.07 TU. Oxygen and hydrogen stable isotopic analyses were performed in the USGS Reston Stable Isotope Laboratory and are reported in per mill (‰) relative to VSMOW (Vienna Standard Mean Ocean Water) and normalized (Coplen 1994) on scales such that the oxygen and hydrogen isotopic values of SLAP (Standard Light Antarctic Precipitation) are –55.5 and –428 ‰, respectively. The reported standard deviation of oxygen and hydrogen isotopic measurements is 0.1 and 1 ‰, respectively.

Water samples taken during September 2010 and analyzed for ^{36}Cl were collected through an in-line filter (disposable; 0.45-μ pore size) into plastic sample containers that were rinsed three times with the filtered water. Analyses of water chemistry and stable isotope data confirmed that, within uncertainties, the September 2010 samples were identical to the earlier March 2010 samples. Measurements of CFCs and SF_6 confirmed that the September 2010 ^{36}Cl samples were not compromised by mixtures with modern water. Six of the seven samples for ^{36}Cl determination had total chloride concentrations of 0.5–1.6 mg L^{-1}. For these, 2 L of water were collected and portions of these were processed chemically (as in Davis et al. 2000) at PRIME Lab, Purdue University, where the targets were prepared and the ^{36}Cl/Cl ratio was determined by AMS procedures (Elmore and Phillips 1987).

Twenty-three sediment samples from six cores in the upper Patapsco Formation of Maryland archived at the Maryland Geological Survey, Baltimore, MD were inspected visually for mineralogy and analyzed by x-ray diffraction. A total of 33 samples including replicates were ground, homogenized, digested in hydrofluoric acid and analyzed for U, Th and Li content using ICPMS.

Results and discussion

Water chemistry

The sampled waters of the upper Patapsco aquifer are relatively dilute (specific conductance, 99–270 μS cm^{-1}, except for sample S-10 where specific conductance increased to about 1,400 μS cm^{-1}). Along the northern flow path the waters are anoxic downgradient from the first well (N-1, dissolved oxygen (DO) 5.4 mg L^{-1}) and DO values decrease downgradient from 0.15 to 0.05 mg L^{-1} (Table 1). Geochemical mass balance calculations using NETPATH (Plummer et al. 1994) indicated possible pyrite oxidation along the upgradient part of the northern flow path, accounting for increases in SO_4^{2-} and Fe^{2+}, followed by sulfate reduction and pyrite formation further downgradient. Small amounts of calcite dissolution and Ca^{2+}/Na^+ exchange account for increases in Na^+, HCO_3^-, and decreases in Ca^{2+}. All waters on the northern flow

 DOI 10.1007/s10040-012-0871-1

path are significantly undersaturated with respect to calcite (saturation index, $SI_c < -1.7$). On the southern flow path the water from the first well (S-1) is anoxic (DO=0.09 mg L^{-1}) and DO values range from 0.04 to 0.16 mg L^{-1} downgradient. NETPATH calculations indicated only minor amounts of Ca^{2+} for Na^{+} cation exchange at the first few wells on the southern flow path, and virtually no reaction further downgradient on the southern flow path. The first sample on the southern flow path is near calcite saturation (S-1, SI_c=–0.22). Further downgradient from S-1, the calcite saturation index ranges from values of –2.0 to –1.2, except at S-10 where the water is saturated with calcite (SI_c=–0.02). NETPATH calculations are uncertain at S-10 but suggest calcite dissolution, addition of CO_2 (perhaps from redox reactions), cation exchange (Ca^{2+} for Na^{+}), and addition of NaCl. The addition of NaCl may indicate leakage from low-permeability zones, upward leakage from aquifers below the upper Patapsco, and/or mixing with paleo seawater along the freshwater–saltwater interface.

The water chemistry of the upper Patapsco aquifer provides little evidence for occurrence of geochemical processes that would adversely affect age interpretation using ^{14}C, ^{4}He accumulation, or ^{36}Cl data. The limited extent of geochemical reactions such as calcite dissolution or oxidation of organic carbon, that can dilute the initial ^{14}C content, indicates that for samples that are on the radiocarbon timescale, application of some of the traditional adjustment models such as that of Fontes and Garnier (1979) or even the conventional radiocarbon age may be appropriate. The low chloride content (except at S-10) indicates little interaction with confining layers or addition of old water with high terrigenic ^{4}He from confining layers. Therefore the waters may be well suited for dating by accumulation of radiogenic ^{4}He, and ^{36}Cl decay, as discussed in the following.

The position of the last glacial maximum (LGM) appears near well N-4 on the northern flow path and is thought to be upgradient of well S-2 on the southern flow path. Dissolved Cl^- concentration along the northern flow path (Table 1) decreases from the recharge zone to a minimum of about 0.53 mg L^{-1} at well N-4, and then increases downgradient from well N-4 (Fig. 5a). On the southern flow path the Cl^- minimum of the LGM is likely between the first and second wells on the flow path, because, as shown in a later section, the apparent age at S-2 indicates the sample is associated with an earlier glacial period. Cl^- concentration along the southern flow path increases downgradient of well S-2 from 0.81 mg L^{-1} (Table 1) to approximately 1.6–1.8 mg L^{-1}. Additional minima in dissolved Cl^- concentration were not detected farther downgradient of the assumed position of the LGM.

The Cl^-/Br^- mass ratio (Table 1) provides a useful indicator of Cl^- source and paleoclimatic conditions (Davis et al. 2004). Recharge of precipitation at the LGM should have a minimum in Cl^-/Br^- mass ratio. Except for sample N-1 and sample S-10, all of the remaining samples have an average Cl^-/Br^- mass ratio of 114±20 which is near the median continental Cl^-/Br^- mass ratio of 101 reported by Davis et al. (2004) for potable groundwater where the Cl^- and Br^- are of atmospheric origin. Along the northern flow path the Cl^-/Br^- mass ratio is 316 at N-1. This sample contains anthropogenic constituents (^{3}H, CFCs), and may also have an excess of anthropogenic Cl^-, such as Cl^- from septic systems (Katz et al. 2011). The Cl^-/Br^- mass ratio along the northern flow path decreased from the recharge zone to a minimum at N-4 (Fig. 5b). Along the southern flow path, the Cl^-/Br^- mass ratio rose only slowly from S-1 to S-4, and then was approximately constant to S-9 (Fig. 5b). The Cl^-/Br^- mass ratio rose steeply to about 240 at S-10, consistent with a dilute seawater source (Fig. 2).

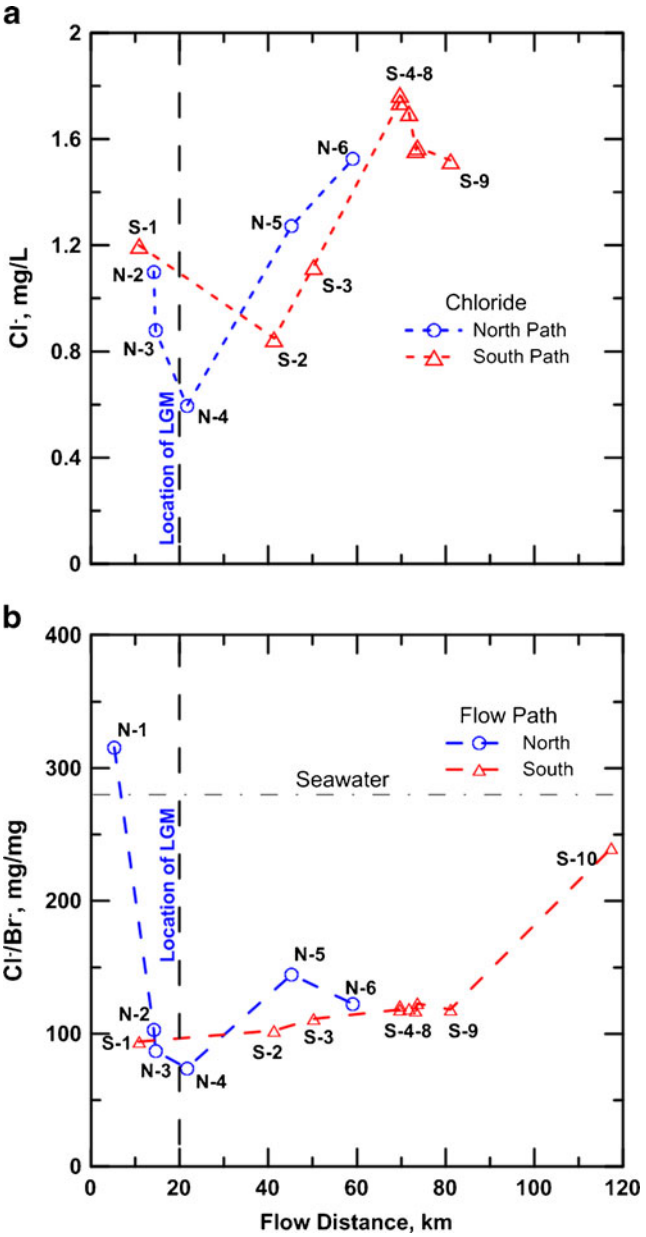

Fig. 5 Variations in **a** Cl^- concentration and **b** the Cl^-/Br^- mass ratio on the northern and southern flow paths of the upper Patapsco aquifer of the Maryland Atlantic Coastal Plain. Values for replicate or re-sampled wells are averaged. Cl^- concentrations for N-1 and S-10 plot at 17.7 and 64.8 mg L^{-1}, respectively

DOI 10.1007/s10040-012-0871-1

Stable isotopes of water

Groundwater along the northern flow path is depleted in stable isotopic composition relative to that along the southern flow path (Table 2, Fig. 6). A plot of waters along the northern flow path, and including samples S-1, S-2, and S-3 on the southern flow path, has a slope that parallels the global meteoric water line (GMWL) (Fig. 6), but is enriched in ^{2}H with a D_{excess} value of approximately 16 ($D_{excess} \equiv \delta^{2}H - 8\delta^{18}O$). This value of D_{excess} is near the maximum D_{excess} value reported by Kendall and Coplen (2001) for any modern surface water in the eastern US. Samples S-4 through S-10 plot below the apparent paleo meteoric water line derived from the northern flow path of $\delta^{2}H = 8\delta^{18}O + 16$ (Fig. 6), suggesting possibly evaporated waters. However, excluding samples N-1 and S-10, the average Cl^{-} concentration on the southern flow path is only slightly elevated relative to that on the northern flow path, 1.45±0.34, and 1.12±0.36 mg L^{-1}, respectively. Therefore, there is not a strong evaporation signal in the dissolved Cl^{-} data. The stable isotope values of the samples on the northern and southern flow paths represent water samples from discrete points in time that span multiple glacial cycles. It is therefore more likely that samples S-4 through S-10 are samples with somewhat lower values of D_{excess} than those of the northern path and of samples S-1 through S-3 on the southern path.

Due to kinetic isotope fractionation, values of D_{excess} are functions of relative humidity over the (oceanic) moisture source (Van der Straaten and Mook 1983; Merlivat and Jouzel 1983). D_{excess} can be elevated in glacial-period moisture (low relative humidity over the moisture source), in comparison to moisture in inter-glacials (high relative humidity). All of the samples of groundwater from the upper Patapsco aquifer have D_{excess} values greater than 10 ‰, consistent with lowered relative humidity in the source area (glacial period moisture). Another factor contributing to stable isotope enrichment during glacial periods follows from the enrichment in stable isotopic composition of the oceans due to loading of isotopically depleted ice on land masses (ice-volume effect) which, for example, increased the $\delta^{18}O$ isotopic composition of precipitation in coastal regions at the LGM by as much as +1.3 ‰. Paleowaters from the LGM in the southeast US were enriched as much as +2.5 ‰ in $\delta^{18}O$ (Plummer 1993). In comparison, samples of Potomac River water collected at Chain Bridge near Washington, DC during 1985–1987 plot along the GMWL (Coplen and Kendall

Table 2 Summary of ^{2}H, ^{18}O, ^{3}H, CFC, SF_6, ^{13}C and ^{14}C data. *ND* not determined

Site no.	$\delta^{2}H$ ‰	$\delta^{18}O$ ‰	D_{excess} ‰	Tritium, TU	Tritium error, TU	CFC-12 pmol kg^{-1} [c]	SF_6 fmol kg^{-1} [d]	$\delta^{13}C$, ‰	^{14}C, pmc	Rept. error 1σ pmc	Conventional ^{14}C age, ka	Adjusted ^{14}C age, ka [e]
N-1	–44.52	–7.31	13.96	6.24	0.22	26.74	0.65	–22.6	110.0	0.34	Mod.	Mod.
N-2	–43.38	–7.34	15.34	0.12	0.07	0.00	0.19	–18.8	17.6	0.12	14.1	15.2
N-3	–44.31	–7.45	15.29	–0.02	0.07	0.00	0.02	–19.0	14.0	0.10	15.9	16.6
N-4	–45.94	–7.81	16.54	–0.01	0.07	0.05	0.05	–17.8	7.0	0.09	21.5	21.5
N-4[a]	–45.92	–7.87	17.04	ND	ND	0.01	0.11	ND	ND	ND	ND	ND
N-5	–47.87	–7.97	15.89	–0.09	0.07	0.00	0.02	–16.0	0.4	0.03	>30	>30
N-5[b]	–48.32	–7.97	15.44	–0.08	0.07	0.00	0.02	–16.1	0.5	0.04	>30	>30
N-5[a]	–47.68	–8.00	16.32	ND	ND	0.01	0.11	ND	ND	ND	ND	ND
N-6	–46.52	–7.83	16.12	–0.04	0.08	0.00	0.04	–15.3	0.3	0.02	>30	>30
N-6[a]	–45.99	–7.75	16.01	ND	ND	0.01	0.15	ND	ND	ND	ND	ND
S-1	–42.32	–7.24	15.60	0.01	0.07	0.01	0.03	–12.4	11.6	0.10	17.5	14.2
S-2	–43.22	–7.36	15.66	0.06	0.07	0.00	0.03	–12.7	0.2	0.02	>30	>30
S-2[a]	–42.89	–7.34	15.83	ND	ND	0.01	0.17	ND	ND	ND	ND	ND
S-3	–41.52	–7.11	15.36	0.09	0.07	0.00	0.11	–13.2	0.2	0.04	>30	>30
S-4	–40.56	–6.91	14.72	0.04	0.07	0.00	0.04	–11.7	0.2	0.02	>30	>30
S-4[b]	–40.76	–6.79	13.56	0.04	0.07	0.00	0.04	–11.7	0.3	0.02	>30	>30
S-4[a]	–40.73	–6.79	13.59	ND	ND	0.01	0.15	ND	ND	ND	ND	ND
S-5	–40.13	–6.81	14.35	–0.02	0.07	0.00	0.02	–11.6	0.6	0.03	>30	>30
S-6	–40.99	–6.83	13.65	0.00	0.07	0.00	0.04	–11.2	0.3	0.02	>30	>30
S-7	–40.80	–6.89	14.32	0.04	0.08	0.00	0.02	–9.5	0.2	0.02	>30	>30
S-8	–41.34	–6.95	14.26	0.00	0.07	0.00	0.03	–9.4	0.4	0.02	>30	>30
S-9	–40.91	–6.98	14.93	0.05	0.07	0.00	0.03	–10.1	0.2	0.03	>30	>30
S-9[a]	–41.58	–6.91	13.70	ND	ND	0.01	0.31	ND	ND	ND	ND	ND
S-10	–41.07	–7.10	15.73	–0.04	0.07	0.00	0.02	–11.0	0.1	0.02	>30	>30
S-10[a]	–41.04	–7.02	15.12	ND	ND	0.00	0.12	ND	ND	ND	ND	ND

[a] Re-sampled for ^{36}Cl analysis

[b] Replicate analysis, QA/QC

[c] ±0.01 pmol kg^{-1}

[d] ±0.05 fmol kg^{-1} . SF_6 is slightly higher in samples collected in Sept. 2010 because they were analyzed in mid-April 2011 6.5 months after collection, which is beyond the normal storage life of the samples. The SF_6 detections are small and attributed to exchange with laboratory air

[e] Fontes and Garnier (1979)

 DOI 10.1007/s10040-012-0871-1

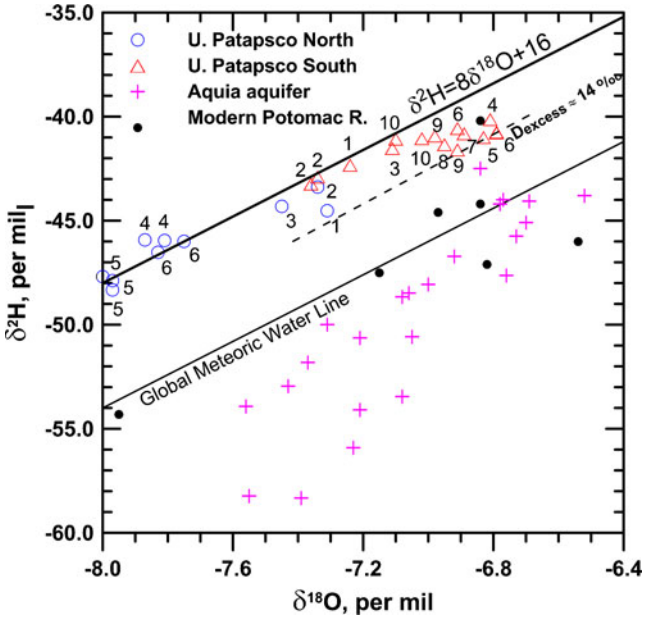

Fig. 6 Deuterium and Oxygen-18 values in water of the northern and southern flow paths in the upper Patapsco aquifer are compared to paleowater from the Aquia aquifer (Aeschbach-Hertig et al. 2002) and modern water from the Potomac River (Coplen and Kendall 2000). Additional samples from Coplen and Kendall (2000) plot to the left of the diagram scattered near the GMWL. Some of the paleowaters from the southern flow path of the upper Patapsco have lower D_{excess} than the depleted paleowaters of the northern flow path. Symbols are *blue* for northern flow path samples and *red* for southern flow path samples. *Numbers* are the abbreviated well numbers from Table 1

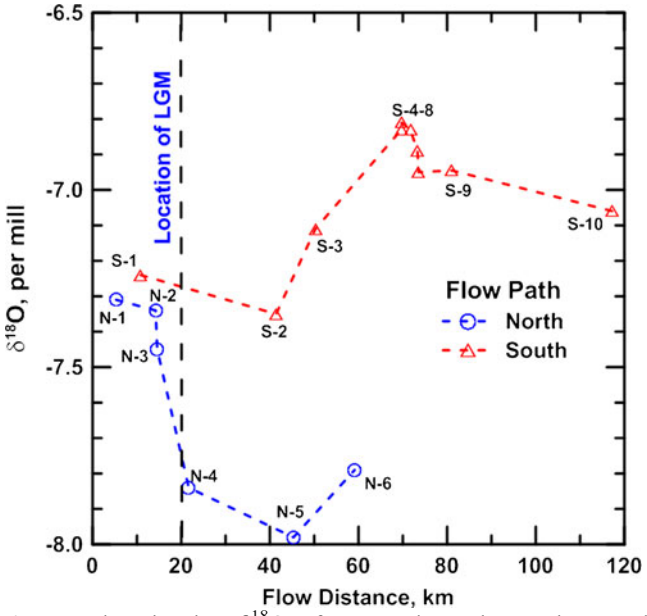

Fig. 7 Plot showing $\delta^{18}O$ of water along the northern and southern flow paths in the upper Patapsco aquifer of Maryland Atlantic Coastal Plain; only the average value of replicate analyses is shown. The location of the LGM at about 20 km downgradient in the upper Patapsco is based on all of the data of this study. The reported one-sigma uncertainty in $\delta^{18}O$ values is±0.1 ‰

2000), with average D_{excess} of 11.5±2.6 ‰ (Fig. 6), unlike the paleowaters.

Stable isotope values also differ significantly with distance of flow between the northern and southern flow directions. The northern flow path shows a distinct minimum in $\delta^{18}O$ at 45 km (N-5) (Fig. 7), which is downgradient of the presumed LGM and is likely associated with an earlier glacial period. Along the southern flow path the minimum $\delta^{18}O$ value is at 41 km (S-2), also downgradient of the likely LGM (Fig. 7). Water samples from further along the southern flow path (S-3–S-10) are elevated in $\delta^{18}O$ relative to samples S-1 and S-2 (Fig. 7), and could represent different extents of ice-volume effect and/or changes in moisture source.

There are notable and unusual differences between the stable isotopic composition of groundwater from the upper Patapsco aquifer and that from the more shallow Aquia aquifer (Aeschbach-Hertig et al. 2002). Many of the Aquia waters plot approximately in the range of $\delta^{18}O$ for the southern flow path upper Patapsco waters (Fig. 6), but have low deuterium values plotting well below the GMWL, in contrast to the upper Patapsco deuterium values that plot significantly above the GMWL. Some of the Aquia aquifer samples of Aeschbach-Hertig et al. (2002) are as depleted in ^{18}O as the upper Patapsco aquifer samples on the northern flow path (Fig. 6), but have low D_{excess} relative to the GMWL and the upper Patapsco samples. Factors that may have altered recharge patterns and stable isotopic composition of the Aquia and upper Patapsco include extent and possible role of permafrost altering recharge patterns in the outcrop zone, and differences in the amounts of infiltration from the ancestral Susquehanna and Potomac Rivers as the paleo river channels crossed the outcrop zones of the upper Patapsco.

Dissolved-gas recharge temperatures and excess air

Comparison of recharge temperatures and quantities of excess air help to explain some apparent differences in recharge processes on the northern and southern flow paths. Table 3 summarizes the N_2–Ar data, N_2–Ar recharge temperatures, and excess air calculated with the UA model. Table 4 lists the noble gas data and Table 5 summarizes the noble-gas recharge temperature (NGRT) calculations. Table 5 also gives the calculated amounts of radiogenic ^4He which are used as an age indicator in a later section of this paper.

There is good agreement between the N_2–Ar (UA model) recharge temperatures and the NGRTs on the northern flow path (Fig. 8a). The agreement is attributed largely to the fact that, although the CE model was applied to the samples, the best fit NGRT was for the case of zero fractionation (F=0) in 5 of the 9 samples on the northern flow path (Table 5). Therefore, for these samples the NGRTs were solved using the UA model as with the N_2–Ar data. The agreement indicates consistency between the GC N_2–Ar data and the MS Ne, Ar, Kr, and Xe data. Recharge temperatures of 10–10.5 °C were found for water at N-1, nearest the recharge zone, which is

DOI 10.1007/s10040-012-0871-1

Table 3 Summary of N_2, Ar, CO_2, and CH_4 data, and UA model recharge temperature and excess air from average N_2–Ar data[a]

Site no.	Average N_2 mg kg^{-1}	N_2 1σ, mg kg^{-1}	Average Ar mg kg^{-1}	Ar 1σ, mg kg^{-1}	Average CO_2 mg kg^{-1}	CO_2 1σ, mg kg^{-1}	Average CH_4 mg kg^{-1}	CH_4 1σ, mg kg^{-1}	N_2–Ar UA model recharge temperature, °C	1σ error in UA model N_2–Ar recharge temperature, °C	N_2–Ar UA model excess air, cm^3 kg^{-1}	N_2–Ar 1σ error in UA model excess air, cm^3kg^{-1}
N-1	20.67	0.18	0.7247	0.0021	76.691	0.058	0.0000	0.0000	10.5	0.5	2.8	0.2
N-2	22.96	0.27	0.8272	0.0076	91.651	1.060	0.0048	0.0000	4.6	0.3	2.6	0.1
N-3	23.25	0.08	0.8417	0.0006	74.971	0.517	0.0040	0.0001	3.5	0.2	2.3	0.2
N-4	24.69	0.03	0.8961	0.0003	49.305	0.013	0.0110	0.0003	1.2	0.1	2.5	0.1
N-4[b]	24.61	0.08	0.9061	0.0017	45.663	0.367	0.0099	0.0001	0.5	0.0	2.0	0.1
N-5	22.88	0.10	0.8189	0.0030	21.557	0.122	0.0118	0.0002	5.1	0.1	2.7	0.0
N-5[b]	22.62	0.08	0.8224	0.0020	22.006	0.226	0.0073	0.0000	4.3	0.1	2.1	0.1
N-6	22.61	0.07	0.8046	0.0029	6.875	0.144	0.0344	0.0047	6.0	0.1	2.9	0.0
N-6[b]	22.54	0.10	0.8080	0.0013	8.292	0.170	0.0094	0.0000	5.5	0.3	2.6	0.2
S-1	20.43	0.25	0.7423	0.0063	7.915	0.015	0.0078	0.0005	8.4	0.2	1.8	0.2
S-2	22.73	0.17	0.8160	0.0041	19.134	0.424	0.0089	0.0005	5.0	0.1	2.5	0.1
S-2[b]	22.74	0.12	0.8230	0.0031	18.508	0.023	0.0074	0.0001	4.5	0.1	2.3	0.1
S-3	22.66	0.10	0.8086	0.0034	2.060	0.030	0.0108	0.0001	5.5	0.2	2.7	0.0
S-4	22.48	0.03	0.7987	0.0022	1.417	0.003	0.0062	0.0001	6.3	0.2	2.9	0.0
S-4[b]	22.39	0.04	0.8030	0.0011	1.557	0.027	0.0060	0.0001	5.7	0.0	2.5	0.0
S-5	22.76	0.00	0.8027	0.0000	1.286	0.000	0.0062	0.0000	6.3	0.1	3.2	0.1
S-6	22.52	0.23	0.7953	0.0071	1.146	0.016	0.0066	0.0001	6.4	0.3	3.0	0.1
S-7	22.56	0.02	0.7995	0.0023	1.083	0.018	0.0066	0.0000	6.4	0.2	3.0	0.1
S-8	22.58	0.17	0.8010	0.0044	1.187	0.009	0.0066	0.0001	6.1	0.1	2.9	0.1
S-9	22.59	0.08	0.7982	0.0024	1.042	0.003	0.0071	0.0001	6.4	0.1	3.0	0.0
S-9[b]	22.57	0.04	0.8053	0.0006	1.034	0.024	0.0069	0.0002	5.8	0.1	2.7	0.1
S-10	21.97	0.10	0.7721	0.0024	3.721	0.020	0.0155	0.0000	8.0	0.1	3.1	0.1
S-10[b]	21.78	0.03	0.7717	0.0011	3.627	0.004	0.0152	0.0001	7.7	0.1	2.8	0.0

[a] All samples were collected and analyzed in duplicate. The tabulated errors are the standard deviation,1σ, of the replicate analyses. Overall, the uncertainties typically are±0.5 °C and 0.5 cm^3 kg^{-1} of water. Analytical uncertainties typically are <1 % for N_2 and Ar, and 1–2 % for CO_2 and CH_4

[b] Re-sampled for ^{36}Cl analysis

DOI 10.1007/s10040-012-0871-1

Table 4 Summary of noble gas data[a]

Site no.	He $cm^3STP\ g^{-1}$	Ne $cm^3STP\ g^{-1}$	Ar $cm^3STP\ g^{-1}$	Kr $cm^3STP\ g^{-1}$	Xe $cm^3STP\ g^{-1}$	R/Ra
N-1	5.779E-08	2.536E-07	4.120E-04	1.095E-07	1.361E-08	2.187
N-2	1.124E-07	2.818E-07	4.753E-04	1.063E-07	1.702E-08	0.569
N-3	1.222E-07	2.609E-07	4.749E-04	1.151E-07	1.907E-08	0.512
N-4	1.427E-07	2.702E-07	5.055E-04	1.246E-07	1.813E-08	0.462
N-4[b]	1.458E-07	2.821E-07	4.987E-04	1.273E-07	1.851E-08	0.459
N-5	5.468E-07	2.591E-07	4.603E-04	1.093E-07	1.574E-08	0.118
N-5[b]	5.477E-07	2.673E-07	4.571E-04	1.129E-07	1.622E-08	0.114
N-6	1.071E-06	2.585E-07	4.650E-04	1.120E-07	1.670E-08	0.066
N-6[b]	1.079E-06	2.691E-07	4.556E-04	1.100E-07	1.615E-08	0.066
S-1	1.020E-07	2.483E-07	4.237E-04	9.989E-08	1.450E-08	0.553
S-2	2.912E-07	2.491E-07	4.425E-04	1.042E-07	1.395E-08	0.208
S-2[b]	2.908E-07	2.625E-07	4.636E-04	1.156E-07	1.576E-08	0.203
S-3	5.352E-07	2.551E-07	4.585E-04	1.105E-07	1.522E-08	0.122
S-4	6.919E-07	2.548E-07	4.478E-04	1.035E-07	1.456E-08	0.101
S-4[b]	6.826E-07	2.641E-07	4.498E-04	1.129E-07	1.543E-08	0.096
S-5	7.413E-07	2.570E-07	4.628E-04	1.173E-07	1.552E-08	0.094
S-5[c]	7.423E-07	2.578E-07	4.688E-04	1.109E-07	1.562E-08	0.092
S-6	7.555E-07	2.605E-07	4.532E-04	1.060E-07	1.492E-08	0.094
S-7	9.663E-07	2.540E-07	4.512E-04	1.101E-07	1.526E-08	0.079
S-8	9.698E-07	2.566E-07	4.611E-04	1.092E-07	1.551E-08	0.081
S-8[c]	9.779E-07	2.580E-07	4.565E-04	1.085E-07	1.541E-08	0.079
S-9	1.178E-06	2.576E-07	4.541E-04	1.118E-07	1.536E-08	0.065
S-9[b]	1.170E-06	2.651E-07	4.494E-04	1.080E-07	1.544E-08	0.064
S-10	8.467E-06	2.557E-07	4.424E-04	1.078E-07	1.502E-08	0.033
S-10[b]	8.606E-06	2.568E-07	4.344E-04	1.053E-07	1.490E-08	0.033
Error	1 %	2 %	2 %	3 %	3 %	1 %
ASW 6, 30.5 m/ 0 ‰	4.717E-08	2.093E-07	4.235E-04	1.021E-07	1.517E-08	0.980
ASW 10, 30.5 m/ 0 ‰	4.628E-08	2.010E-07	3.847E-04	9.070E-08	1.313E-08	0.980

[a] Mass spectrometric analyses: Concentrations in cm^3 STP per gram of water (cm^3 STP g^{-1}) ASW 6, 30.5 m/ 0 ‰, air-saturated water at 6 °C, 30.5 m elevation and salinity of 0 parts per thousand. ASW 10, 30.5 m/ 0 ‰, air-saturated water at 10 °C, 30.5 m elevation and salinity of 0 parts per thousand

[b] Re-sampled for ^{36}Cl analysis

[c] Replicate analysis, QA/QC

2.5–3.0 °C colder than the approximate mean annual temperature of 13.0 °C.

A minimum recharge temperature at well N-4 on the northern flow path likely locates the position of recharge from the LGM in the upper Patapsco. Well N-4 was sampled twice over a 6-month period, yielding NGRTs of 1.3–1.5 °C and N_2–Ar recharge temperatures of 1.2–0.5 °C between the March and September, 2010 samplings, respectively. Upgradient of the LGM on the northern flow path, calculated recharge temperatures are higher in younger recharge, while downgradient of the LGM older waters show recharge temperatures of 4–6 °C (Fig. 8a).

The position of the LGM on the southern flow path likely is at a flow distance of 20 km, as on the northern flow path, but is not clearly delineated due to inadequate sample density on the southern flow path. This conclusion is based on a calculated age of approximately 150 ka for water at S-2, indicating that the minimum in stable isotopic composition at S-2 represents an earlier (Illinoian) glacial period. The lowest recharge temperatures on the southern flow path range from 4.5–5.0 °C (N_2–Ar) to 5.1 °C (NGRT), (Fig. 8b).

Amounts of UA-model N_2–Ar excess air are nearly identical for the northern and southern flow paths, averaging 0.0025±0.0003 $cm^3STP\ g^{-1}$ and 0.0027± 0.0004 $cm^3STP\ g^{-1}$ respectively. In applying the CE model, five of the nine samples were fitted to the UA model on the northern flow path, and seven of the 16 samples analyzed on the southern flow path were solved as unfractionated (Table 5). Overall, the A_e parameter of the CE model (initial trapped air volumes), averaged 0.0057 $cm^3STP\ g^{-1}$ for waters on the northern flow path and 0.0123 $cm^3STP\ g^{-1}$ on the southern flow path, indicating more than twice as much excess air was initially trapped and subsequently fractionated on the southern flow path than on the northern flow path. The higher amounts of A_e on the southern flow path are consistent with infiltration from ponded water, presumably within the Potomac River basin (see later discussion).

Groundwater age estimates

Apparent ages of groundwater were estimated from measurements of ^{14}C, ^{36}Cl and ^{4}He. All the tracers show groundwater age increasing systematically with increasing flow distance (Fig. 9).

Radiocarbon ages

Along both the northern and southern flow paths, ^{14}C concentrations decreased below the interpretable range (30 ka) within the first 40 km of flow in the upper Patapsco (Fig. 9 and Table 2). Only 5 of the 16 wells sampled for ^{14}C had concentrations that were greater than

 DOI 10.1007/s10040-012-0871-1

Table 5 Summary of noble gas recharge temperatures and amounts of radiogenic ^{4}He

Site no.	EA model	NGRT °C	± Error °C	Ae cm^3 STP g^{-1} [c]	± 1σ Ae cm^3 STP g^{-1}	EA cm^3 STP g^{-1}	± 1σ EA cm^3 STP g^{-1}	*F*	± 1σ *F*	X^2 ceiling[d]	X^2	ΔNe (% solubility)	± 1σ ΔNe (%)	Radiogenic ^{4}He cm^3 STP g^{-1}	± 1σ Radiogenic ^{4}He cm^3 STP g^{-1}
N-1	UA	10.0	0.7			0.0029	0.0003			3.84	0.00	26.1	2.79	ND	ND
N-2	UA	3.9	0.6			0.0037	0.0003			3.84	0.70	31.2	2.90	4.539E-08	1.990E-09
N-3	UA	3.3	0.7			0.0025	0.0003			3.84	0.16	20.9	2.78	6.138E-08	2.043E-09
N-4	CE	1.5	1.4	0.0081	0.0981	0.0032	0.0011	0.535	0.325	3.84	0.82	22.8	3.05	8.095E-08	2.286E-09
N-4[a]	CE	1.3	0.6	0.0033	0.0044	0.0033	0.0004	0.000	0.128	3.84	3.01	27.3	2.81	7.995E-08	2.225E-09
N-5	CE	5.4	1.3	0.0081	0.0742	0.0031	0.0009	0.546	0.323	3.84	0.20	23.0	2.99	4.865E-07	5.806E-09
N-5[a]	UA	5.1	0.6			0.0030	0.0003			3.84	0.56	26.1	2.84	4.844E-07	5.789E-09
N-6	UA	4.3	0.5			0.0025	0.0003			5.99	0.00	21.4	2.70	1.010E-06	1.072E-08
N-6[a]	CE	5.1	0.6	0.0031	0.0116	0.0031	0.0004	0.000	0.149	3.84	0.93	26.9	2.84	1.015E-06	1.073E-08
S-1	CE	7.8	0.8	0.0023	0.0307	0.0023	0.0005	0.000	0.141	3.84	0.25	20.7	2.72	4.301E-08	1.759E-09
S-2	UA	6.2	0.7			0.0022	0.0003			3.84	0.00	19.0	2.73	2.324E-07	3.347E-09
S-2[a]	UA	5.1	0.6			0.0028	0.0003			3.84	0.32	24.5	2.87	2.285E-07	3.363E-09
S-3	CE	6.4	2.2	0.0233	0.1627	0.0037	0.0012	0.728	0.282	3.84	1.58	22.3	3.51	4.766E-07	5.550E-09
S-4	UA	6.9	0.6			0.0027	0.0003			3.84	1.59	23.5	2.78	6.309E-07	7.012E-09
S-4[a]	UA	6.1	0.7			0.0030	0.0003			3.84	0.02	26.2	2.80	6.197E-07	7.015E-09
S-5	UA	5.3	0.0			0.0026	0.0000			3.84	1.06	22.3	0.00	6.804E-07	0.000E+00
S-5[b]	CE	6.2	2.1	0.0271	0.1446	0.0040	0.0012	0.729	0.241	3.84	0.00	23.5	3.50	6.831E-07	7.633E-09
S-6	CE	7.1	1.8	0.0158	0.0970	0.0039	0.0010	0.647	0.276	3.84	0.32	25.9	3.18	6.949E-07	7.807E-09
S-7	CE	5.9	1.7	0.0090	0.1276	0.0029	0.0010	0.601	0.336	3.84	1.83	21.2	3.09	9.073E-07	9.603E-09
S-8	CE	5.9	1.7	0.0166	0.1154	0.0035	0.0010	0.688	0.298	3.84	0.35	22.5	3.09	9.107E-07	9.660E-09
S-8[b]	CE	5.9	1.6	0.0089	0.1011	0.0032	0.0010	0.568	0.309	3.84	0.00	23.2	3.06	9.178E-07	9.926E-09
S-9	UA	5.8	0.6			0.0027	0.0003			3.84	0.28	23.1	2.78	1.116E-06	1.204E-08
S-9[a]	CE	5.9	0.9	0.0030	0.0319	0.0030	0.0006	0.000	0.224	3.84	0.60	26.4	2.84	1.107E-06	1.181E-08
S-10	UA	6.5	0.7			0.0026	0.0003			3.84	0.00	22.9	2.71	8.406E-06	8.475E-08
S-10[a]	CE	6.8	0.9	0.0027	0.0345	0.0027	0.0005	0.000	0.171	3.84	1.18	23.5	2.78	8.545E-06	8.620E-08

EA excess air; *NGRT* noble gas recharge temperature; *Ae* excess air parameter for CE model; *F* fractionation factor in CE excess air model; *ΔNe* neon in excess of solubility equilibrium in percent. Model parameters: Elevation 30.5 ± 10 m; Salinity 0 per mil. Excess air (EA) for CE models computed from recharge parameters assuming oxygen-saturated waters. See text for additional information

[a] Re-sampled for ^{36}Cl analysis

[b] Replicate analysis, QA/QC

[c] UA model, Ae, can be compared to excess air from N_2–Ar data, Table 3, by multiplying Ae by 1,000

[d] X^2 ceiling based on degrees of freedom and a probability of 0.05

DOI 10.1007/s10040-012-0871-1

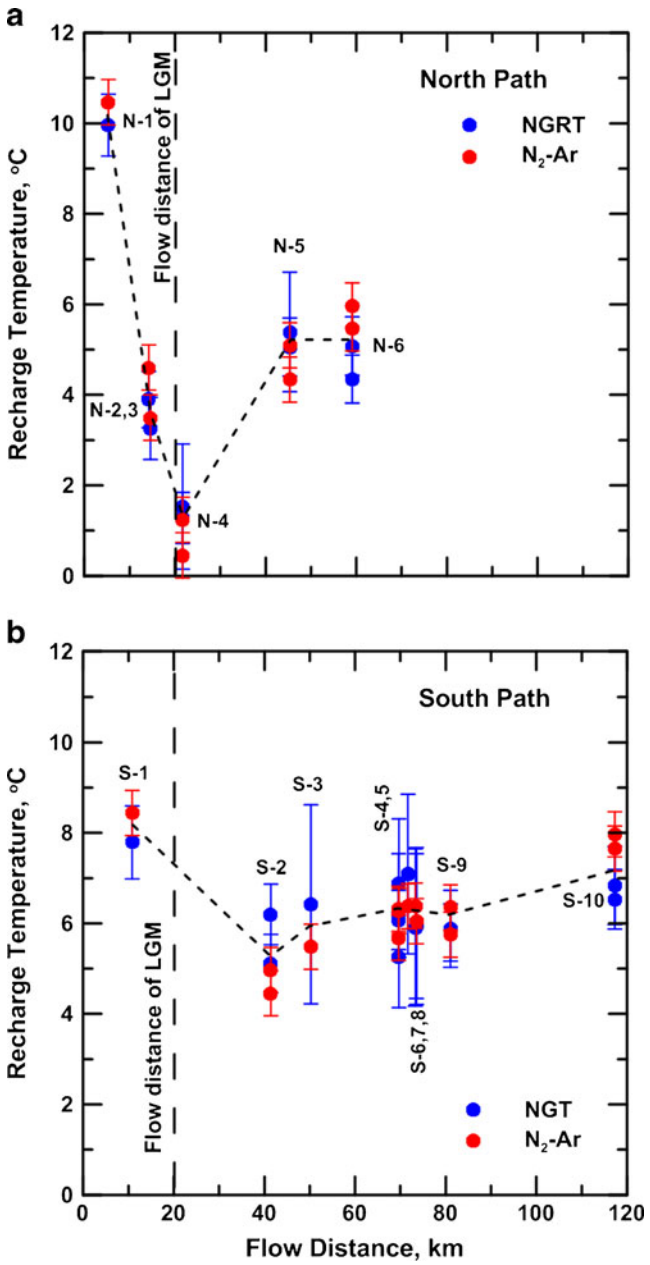

Fig. 8 Comparison of recharge temperatures calculated from noble gas data and N_2–Ar data along **a** the northern flow path of the upper Patapsco, and **b** the southern flow path of the upper Patapsco. On the northern flow path, the recharge temperatures decrease from a value near the mean annual temperature in the recharge zone (13 °C) to the range of 0.5–1.5 °C at N-4 which represents water recharged at the LGM. On the southern flow path, the recharge temperatures decrease from a value near 8 °C in the recharge zone to values near 5 °C at S-2 which likely represents water recharged prior to the LGM

0.5 pmc, and one of these (N-1) was considered modern as the sample contains tritium (6.24 TU), detectable CFCs, and elevated ^{14}C content (109.95 pmc; Table 2). The DIC from the four other samples (N-2, N-3, N-4, and S-1) was radiocarbon dated (Table 2). Two radiocarbon ages were calculated for each sample: (1) the conventional radiocarbon age, and (2) an adjusted age using the model of Fontes and Garnier (1979). Calculations made using NETPATH showed that the waters were little affected by water–rock reactions and those reactions that did occur (pyrite oxidation utilizing dissolved oxygen from the recharge zone and cation exchange) had a neglible effect on the ^{14}C content of the DIC. Of all the samples, only S-1 is near calcite saturation (SI_c=–0.2), and contains elevated Ca^{2+} (40.1 mg L^{-1}), which accounts for the lower adjusted ^{14}C age relative to the conventional ^{14}C age at S-1 (Table 2). X-ray diffraction analysis of 23 samples from the six upper Patapsco cores detected traces of calcite in two samples and NETPATH calculations showed little evidence of oxidation of lignite and/or DOC, reactions that could affect the ^{14}C content. The ^{14}C ages from the Fontes and Garnier (1979) model were adopted in this study because they appear to improve the ^{14}C age estimate of DIC at well S-1. The adjusted radiocarbon ages are consistent with (1) the stable isotope data (Fig. 7), (2) location of the Cl^- and Cl^-/Br^- mass ratio minima (Fig. 5), and (3) location of minima in paleorecharge temperatures (Fig. 8) that indicate the LGM occurs near N-4 and upgradient of S-2.

^{36}Cl ages

The $^{36}Cl/Cl$ ratio decreased systematically downgradient along both the northern and southern flow paths in the upper Patapsco aquifer (Fig. 9), indicating increased age with flow distance. There are several processes to consider when interpreting ^{36}Cl ages from the data (Table 6): (1) definition of the initial, pre-bomb $^{36}Cl/Cl$ ratio in groundwater recharged to the aquifer that accounts for the combined sources of cosmogenic ^{36}Cl in precipitation and hypogenic ^{36}Cl dissolved from mineral surfaces in the recharge area (Bentley et al. 1986; Phillips et al. 1986; Balderer and Synal 1996; Phillips 2000), (2) additional in-situ sources of ^{36}Cl in the upper Patapsco aquifer, (3) diffusion of very old Cl^- from confining layers (presumably of marine origin) and (4) the possibility of the $^{36}Cl/Cl$ ratio in recharge changing over time.

An initial $^{36}Cl/Cl$ ratio of 340×10^{-15} was assumed for pre-bomb water recharging the upper Patapsco based on the measured value of 323×10^{-15} at N-4 and selected previously published values (Purdy et al. 1996; Davis et al. 1998, Moysey et al. 1999; Davis et al. 2000; Moysey et al. 2003; Davis et al. 2003). Given the relatively smooth decrease in $^{36}Cl/Cl$ ratio with flow distance (Fig. 9), it is likely that any remnant of marine Cl^- from intermittent zones of low-permeability sediment present in the upper Patapsco has been flushed from the Cretaceous sands. This conclusion is also supported by the relatively low Cl/Br ratios (Table 1) in all samples except at the end of the southern flow path (S-10) and the smooth variations in Cl^- and Cl/Br with flow distance in the aquifer (Fig. 5).

The evolution of ^{36}Cl in the upper Patapsco aquifer was interpreted according to the mass-balance model of Bentley et al. (1986) and Phillips et al. (1986) (Eq. 1) which accounts for (1) decay of the initial ^{36}Cl that is of meteoric (cosmogenic) or hypogenic origin in recharge, (2) addition of ^{36}Cl from deep subsurface nucleogenic

 DOI 10.1007/s10040-012-0871-1

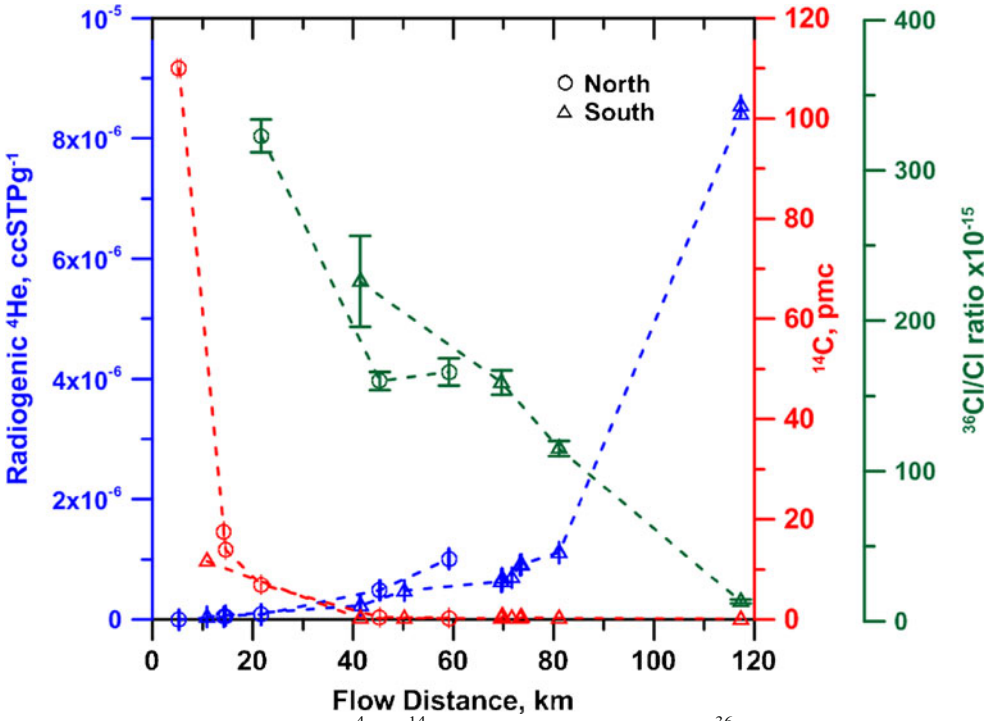

Fig. 9 Comparison of concentrations of radiogenic ^{4}He, ^{14}C of DIC and values of the ^{36}Cl/Cl ratio with distance of flow along the northern and southern flow paths in the upper Patapsco aquifer

production and (3) addition of sedimentary Cl^- (e.g. leakage from confining layers, rock weathering, halite dissolution, etc.),

$$^{36}\mathrm{Cl} = \mathrm{RC} = R_o C_o e^{-\lambda_{36} t} + R_{se} C_o (1 - e^{-\lambda_{36} t}) + R_{se}(C - C_o), \quad (1)$$

where ^{36}Cl is the concentration of ^{36}Cl in the sample, R is the measured ^{36}Cl/Cl ratio, C is Cl^- concentration, R_o is the initial ^{36}Cl/Cl ratio of the total dissolved Cl^- recharged to the aquifer, C_o is the initial Cl^- concentration, R_{se} is the ^{36}Cl/Cl ratio in the aquifer and confining layer(s) at secular equilibrium, and λ_{36} is the ^{36}Cl decay constant ($\lambda_{36} \equiv \ln 2/t_{1/2} a^{-1}$, where $t_{1/2}$ is the ^{36}Cl half-life, 301,000± 4,000 years). Solving Eq. 1 for time, the ^{36}Cl age is (Bentley et al. 1986; Phillips et al. 1986)

$$t = -(1/\lambda_{36}) ln[C(R - R_{se})/C_o(R_o - R_{se})] \quad (2)$$

Equation (2) was applied to calculate age of the six low-chloride samples (N-4, N-5, N-6, S-2, S-4, S-9), with the assumption that $C=C_o$. Equation (2) also was applied to sample S-10 where there is clear evidence for an additional source of Cl^- as well as recharge. A Cl^- concentration in recharge, C_o, of 1.19 mg L^{-1} was calculated as the average of the six low-Cl^- concentrations and applied to sample S-10. The value of R_{se} is expected to be low so values of 12×10^{-15}, 11×10^{-15} and 5×10^{-15}, similar to those calculated for typical shale and sandstone compositions (Bentley et al. 1986), were used (Table 6). Uncertainties in ^{36}Cl ages were calculated using the analytical uncertainty (Table 6), and are insensitive to the selected range in R_{se} values for the six low-Cl^- samples.

The ^{36}Cl ages range from 23 to 328 ka on the northern flow path and 185 to 503 ka on the southern flow path (excluding sample S-10). Considering the analytical uncertainties, the maximum ^{36}Cl ages are 364 ka on the northern flow path and 525 ka on the southern flow path (Table 6). The ^{36}Cl age range for S-10 cannot be determined because the sample appears near secular equilibrium, which would indicate an age of probably more than 2 Ma (Phillips 2000).

Radiogenic ^{4}He accumulation rate and ^{4}He ages

Groundwater ages were estimated from the measured radiogenic ^{4}He in water samples using an estimated radiogenic ^{4}He accumulation rate. Radiogenic ^{4}He is produced by α-decay of U-Th series nuclides (Andrews and Lee 1979; Torgersen and Clarke 1985; Stute et al. 1992; Aeschbach-Hertig et al. 2002) and enters groundwater by (1) in-situ production within the aquifer sediment, (2) diffusional flux from fresh mineral grains (Solomon et al. 1996), and (3) flux from adjacent aquifers or the underlying mantle. Using the noble gas data of Table 4, and excluding sample N-1 which contains tritium and tritiogenic ^{3}He, a plot of the ^{3}He/^{4}He ratio, R, as a function of Ne/^{4}He indicates an average value of R for the radiogenic component, R_{rad}, of 2.2×10^{-8} in the upper Patapsco samples. Values of R_{rad} differ slightly with flow path, averaging 1.2×10^{-8} for the northern flow path and 2.7×10^{-8} for the southern flow path. Fits to the data of Aeschbach-Hertig et al. (2002) lead to somewhat lower

 DOI 10.1007/s10040-012-0871-1

Table 6 Summary of ^{36}Cl ages

Site no.	^{36}Cl/Cl $\times 10^{-15}$	^{36}Cl/Cl error in reporting unit	^{36}Cl$^-$ conc. (atoms L^{-1})$\times 10^6$	^{36}Cl$^-$ error (atoms L^{-1})$\times 10^6$	R_{se} 5×10^{-15} ^{36}Cl age, ka (Eq. 2)[a]	5×10^{-15} Age range, ka[a]	11×10^{-15} ^{36}Cl age, ka (Eq. 2)[a]	11×10^{-15} Age range, ka[a]	12×10^{-15} ^{36}Cl age, ka (Eq. 2)[a]	12×10^{-15} Age range, ka[a]	U-Th ^{4}He implied initial ^{36}Cl/Cl ratio[b]	^{14}C-calib. implied initial ^{36}Cl/Cl ratio[c]	^{36}Cl implied ^{4}He accum. rate, cm^3 STP g^{-1} year^{-1} ($\times10^{-12}$)[d]
N-4	323	11	2.91	0.09	22.6	8–38	23.0	8–39	23.1	8–39	344	340	3.46
N-5	160	6	3.29	0.13	335	318–352	344	327–362	346	328–364	233	218	1.40
N-6	166	9	4.20	0.23	318	295–343	327	302–353	328	304–354	367	318	3.09
S-2	226	30	3.11	0.23	180	125–244	185	127–250	185	128–251	271	262	1.24
S-4	159	8	4.43	0.22	337	315–361	347	324–371	349	326–373	257	236	1.78
S-9	115	5	2.89	0.14	484	464–504	500	480–522	503	482–525	268	232	2.20
S-10	13	1.3	14.42	1.11	ND[e]	ND[e]	442	240–830	704	385–>700	ND[e]	ND[e]	12.14

[a] Initial ^{36}Cl/Cl ratio$\equiv340\times10^{-15}$

[b] Initial ^{36}Cl/Cl ratio implied by the ^{14}C-calibrated ^{4}He age for $R_{se}=12\times10^{-15}$

[c] Initial ^{36}Cl/Cl ratio implied by the U-Th ^{4}He age for $R_{se}=12\times10^{-15}$

[d] ^{4}He accumulation rate calculated from amount of radiogenic ^{4}He and ^{36}Cl age, R_{se} of 12×10^{-15}

[e] Not possible, or negative age results

values of R_{rad} for the Aquia, on the order of 0.9×10^{-8}. As helium of mantle origin can have R values three orders of magnitude greater that R_{rad} (Ozima and Podosek 1983), a mantle source of helium can be excluded for the upper Patapsco (and Aquia) samples. The diffusional flux of ^{4}He from mineral grains in the upper Patapsco sands is expected to be small because of the relatively old (Cretaceous) age of the aquifer material. Further, there is no evidence for a deep crustal flux of ^{4}He, except possibly at sample S-10.

The in-situ radiogenic ^{4}He accumulation rate, A_{He}, was then calculated from measurements of U and Th in the upper Patapsco aquifer sands according to Eq. 3 (Stute et al. 1992, as modified from Andrews and Lee 1979),

$$A_{He} = \Lambda_{He}\frac{\rho_r}{\rho_w}(C_U P_U + C_{Th}P_{Th})\frac{1-n}{n_{eff}} \quad (3)$$

where Λ_{He} is the release factor (assumed equal to 1 following Aeschbach-Hertig et al. 2002), ρ_r and ρ_w are density of rock (taken as 2.6 g cm^{-3}) and water; and C_U and C_{Th} are concentrations of U and Th in the upper Patapsco sediment, μg g^{-1}. The ^{4}He production rates from U and Th decay are assumed to be, $P_U=1.19\times10^{-13}$ cm^{3}STP μg$_U^{-1}$ a^{-1} and $P_{Th}=2.28\times10^{-14}$ cm^{3}STP μg$_{Th}^{-1}$ a^{-1} (following Aeschbach-Hertig et al. 2002).

The lithology of samples from six cores in the upper Patapsco of the Maryland Atlantic Coastal Plain (Fig. 1) was predominantly sand, silt and clay with some gravel. The mineralogy was predominantly quartz, and clay minerals (varying amounts of kaolinite and smectite), with occasional traces of calcite, FeOOH, lignite, gypsum, K-feldspar, and plagioclase feldspar. Clastic grains typically are coated with FeOOH. Twenty-six analyses of U and Th concentrations in the sediment in 13 separate samples from the 6 upper Patapsco cores averaged 1.9±1.2, and 7.5±5.3 μg g^{-1}, respectively. Using values of total porosity, n, and effective porosity, n_{eff} , from measurements on Aquia aquifer sediment (Hansen 1977), n=0.39±0.02; n_{eff}=0.25±0.02, the average radiogenic ^{4}He accumulation rate (Eq. 3) for the upper Patapsco is (2.8±1.8)$\times10^{-12}$ cm^{3}STP g^{-1} a^{-1}. A similar application to eight analyses from five samples that were from the base of the Magothy, the clay-rich top of the Patapsco, or the clay-rich middle-confining layer of the Patapsco formation yielded average U and Th contents of 4.4±2.9 and 9.2±5.8 μg g^{-1}, respectively, and an average ^{4}He accumulation rate of (5.0±2.4)$\times10^{-12}$ cm^{3}STP g^{-1} a^{-1}. Hansen and Wilson (1984) reported values of n=0.42 and n_{eff}=0.36 for the upper Patapsco in a core near well S-9. Using Eq. (3), these values lead to lower radiogenic ^{4}He accumulation rates for the upper Patapsco (1.9±1.1)$\times10^{-12}$ cm^{3}STP g^{-1} a^{-1}) that may be more appropriate for the southern extent of the southern flow path, but lead to ^{4}He ages that are older than expected at the position of the LGM (N-4), approximately 21 ka on the northern flow path. It was concluded that the porosity data from Hansen and Wilson (1984) are not representative of the upper Patapsco

DOI 10.1007/s10040-012-0871-1

throughout the study area and, therefore, the porosity values measured in the Aquia of Hansen (1977) were applied to the upper Patapsco. Eleven additional analyses of U and Th in sediment from the upper Patapsco core AA Bf 100 located near wells N-2 and N-3 (Duigon and Bolton 2003) yield an average ^{4}He accumulation rate of $(2.4\pm1.3)\times10^{-12}$ cm^{3}STP g^{-1} a^{-1}, which is within the uncertainty of the average ^{4}He accumulation rate obtained in this study.

Applying the average U-Th derived radiogenic ^{4}He accumulation rate for the upper Patapsco of $(2.8\pm1.8)\times10^{-12}$ cm^{3}STP g^{-1} a^{-1} to the determined amounts of radiogenic ^{4}He (Table 5), the ^{4}He ages increase on both flow paths to values approaching the range of 300–400 ka (Fig. 10). The oldest water at the farthest point downgradient of the southern flow path, S-10, has a U-Th based ^{4}He age of about 3 Ma, with a range of 1.8–8.4 Ma (Fig. 10), using the measured range in the U-Th content in the sediment cores.

The large error bars associated with the radiogenic ^{4}He ages (Fig. 10) are a consequence of the relatively large standard deviation of the U and Th analyses that are based on complete digestion and analysis of separate sediment samples. The large error bars seem inconsistent with the smooth increase in radiogenic ^{4}He concentration with distance of flow. As the clastic sediment (primarily quartz) of the upper Patapsco is nearly non-reactive, ^{4}He produced within mineral grains may not be the primary source of the measured radiogenic ^{4}He in the upper Patapsco. A possibility, that was not investigated, is that the radiogenic ^{4}He may be derived from decay of relatively uniform concentrations of U and Th that may be adsorbed or incorporated within FeOOH coatings on mineral grains. FeOOH coatings on mineral grains are abundant throughout the upper Patapsco, and dissolved U concentrations typically were below detection by ICPMS analysis (<0.01 μg L^{-1}) in the reducing groundwater. Groundwater in exchange equilibrium with FeOOH coatings may result in relatively uniform concentrations of U and Th on mineral surfaces in contact with groundwater of the upper Patpasco. The result may be lowered standard deviations in radiogenic ^{4}He production rate and in radiogenic ^{4}He ages.

^{14}C-calibrated radiogenic ^{4}He accumulation rates

The four radiocarbon ages (Table 2) were combined with radiogenic ^{4}He content to estimate empirical, ^{14}C-calibrated ^{4}He accumulation rates. The average, empirical ^{14}C-calibrated ^{4}He accumulation rate is $(3.4\pm0.6)\times10^{-12}$ cm^{3}STP g^{-1} a^{-1} using the adjusted ages derived from the ^{14}C adjustment model of Fontes and Garnier (1979). An advantage of using accumulation of radiogenic ^{4}He as an age indicator is that ^{4}He concentration increases with age, making it easily detectible in old water, as compared to radioactive tracers that decrease in concentration with age. However, there can be large uncertainties in ^{4}He ages if the accumulation rate varies in an unknown way with distance of flow or if additional sources of ^{4}He are not quantified.

The ^{14}C-calibrated ^{4}He ages are similar on the northern and southern flow paths for flow distances less than 50 km (Fig. 11). Table 7 compares the U-Th radiogenic ^{4}He ages and the ^{14}C-calibrated radiogenic ^{4}He ages for the upper

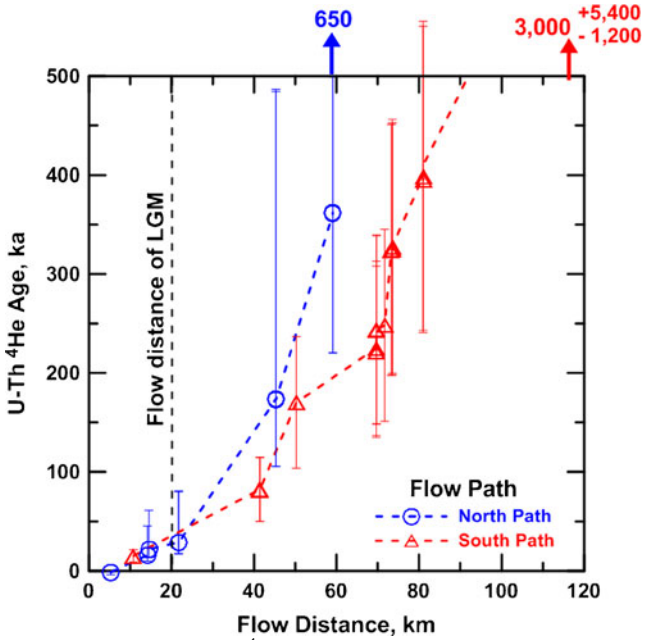

Fig. 10 Comparison of ^{4}He accumulation ages for waters on the northern and southern flow paths of the upper Patapsco based on the average calculated U-Th radiogenic ^{4}He accumulation rate for the upper Patapsco. The *error bars* are based on the standard deviation of ^{4}He accumulation rates calculated from the 26 measurements of U and Th in upper Patapsco sediment of the Maryland Atlantic Coastal Plain

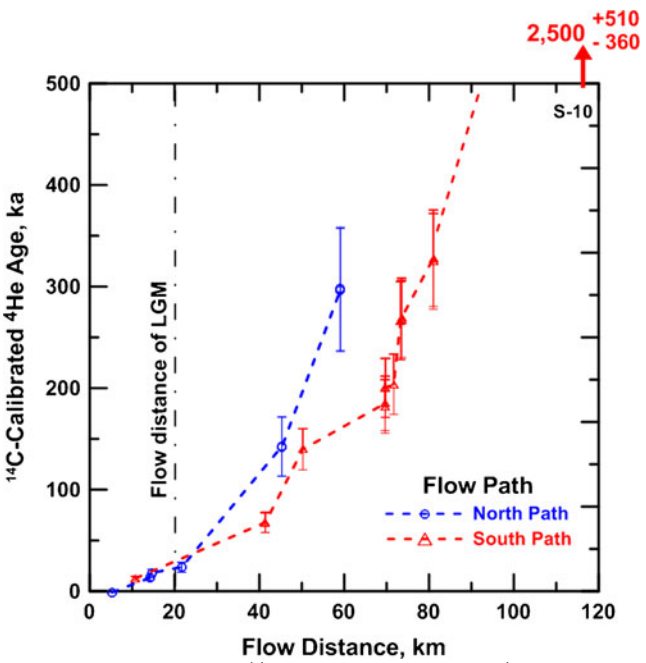

Fig. 11 Comparison of ^{14}C-calibrated radiogenic ^{4}He accumulation ages for waters on the northern and southern flow paths of the upper Patapsco. The *error bars* are based on the standard deviation of the ^{14}C-calibrated radiogenic ^{4}He accumulation rate

DOI 10.1007/s10040-012-0871-1

Table 7 Summary of average ^{4}He accumulation ages, upper Patapsco aquifer

Site no.	^{4}He age from average U-Th radiogenic ^{4}He accumulation rate $(2.8\pm1.8)\times10^{-12}$ cm^{3}STP g^{-1} a^{-1}		^{4}He age from average ^{14}C-calibrated radiogenic ^{4}He accumulation rate $(3.4\pm0.6)\times10^{-12}$ cm^{3}STP g^{-1} a^{-1}		^{14}C implied ^{4}He accumulation rate cm^{3}STP g^{-1} a$^{-1}\times10^{-12}$
	ka	Age range, ka	ka	Age range, ka	
N-1	ND	ND	ND	ND	ND
N-2	16	10–45	13	11–16	3.22
N-3	22	13–61	18	15–22	3.86
N-4	29	18–81	24	20–29	3.76
N-4[a]	29	17–80	23	20–28	3.72
N-5	174	106–486	143	122–172	ND
N-5[a]	173	105–484	142	122–171	ND
N-6	361	220–1,010	297	254–357	ND
N-6[a]	362	221–1,020	298	255–358	ND
S-1	15	9–43	13	11–15	2.48
S-2	83	50–231	68	58–82	ND
S-2[a]	82	50–230	67	58–81	ND
S-3	170	104–476	140	120–168	ND
S-4	225	137–630	185	158–223	ND
S-4[a]	222	135–620	182	156–219	ND
S-5	243	148–682	200	171–241	ND
S-5[b]	244	149–683	200	171–241	ND
S-6	248	151–695	204	174–245	ND
S-7	324	197–907	266	228–321	ND
S-8	325	198–911	267	228–322	ND
S-8[b]	328	200–918	269	230–324	ND
S-9	399	243–1,110	328	280–395	ND
S-9[a]	395	241–1,100	325	278–391	ND
S-10	3,000	1,800–8,400	2,467	2,100–3,000	ND
S-10[a]	3,050	1,900–8,500	2,507	2,100–3,000	ND
				Average	3.4±0.6

[a] Re-sampled for ^{36}Cl analysis

[b] Replicate analysis, QA/QC

Patapsco. Some consistency is evident in the derived ages because (1) the ages are similar and increase smoothly with distance of flow on both flow paths, indicating that the ^{14}C-calibrated ^{4}He accumulation rate remains relatively constant through approximately the first 50 km of flow in the upper Patapsco aquifer, and (2) even over a relatively short flow-length of 4 km on the southern flow path (at 70–74 km for S-4 to S-8), the ages continue to increase with distance of flow for all five wells at this location (Fig. 11).

The ^{14}C-calibrated ^{4}He accumulation rate indicates that the age of water at S-10 is on the order of 2.5 Ma. Water from S-10, at the end of the southern flow path contains 65 mg L^{-1} Cl^{-}, compared to values of 0.5–1.8 mg L^{-1} for all the other samples (Table 1). The source for the elevated Cl^{-} in the upper Patapsco at this location likely is older than the low-Cl^{-} freshwater recharge fraction and likely is elevated in radiogenic ^{4}He. Therefore, the age of 2.5 Ma derived from the empirical ^{14}C-calibrated radiogenic ^{4}He accumulation rate at S-10 may overestimate the age of the recharge fraction in the sample. Excluding sample S-10, the ^{14}C-calibrated ^{4}He accumulation ages of the oldest waters appear to be at N-6 on the northern flow path (298 ka, range 255–358 ka) and at S-9 on the southern flow path (325 ka, range 278–391 ka). In comparison, the average U-Th radiogenic ^{4}He ages are 362 ka (range 221–1,021 ka) at N-6, and 395 ka (range 241–1,100 ka) at S-9 (Table 7).

Comparison of ^{36}Cl and U-Th radiogenic ^{4}He ages

The ^{36}Cl ages (Table 6) can be compared to the U-Th radiogenic ^{4}He ages, and the ^{14}C-calibrated radiogenic ^{4}He accumulation ages (Table 7) and their age ranges (Tables 6 and 7). The comparatively wide error bars of the ^{4}He ages generally overlap the ^{36}Cl age ranges, but 2 samples have poorer agreement in ^{36}Cl and ^{4}He ages (N-5 and S-2) (Tables 6 and 7). All ^{36}Cl ages in Table 6 assume an initial ^{36}Cl/Cl ratio of 340×10^{-15}.

Using the ^{4}He ages and measured ^{36}Cl/Cl ratio, the value of the initial ^{36}Cl/Cl ratio needed for agreement between the ^{36}Cl and ^{4}He ages was calculated for the U-Th radiogenic ^{4}He accumulation ages and the ^{14}C-calibrated ^{4}He accumulation ages (Table 6). Initial ^{36}Cl/Cl ratios of $233–344\times10^{-15}$ are implied, with 4 values lower than the assumed initial ratio of 340×10^{-15} and closer to those suggested by Moysey et al. (2003) and Davis et al. (2003). Therefore, one explanation for differences in ^{36}Cl and ^{4}He ages could be differences in the initial ^{36}Cl/Cl ratio recharged to the upper Patapsco aquifer with time. Indeed, the highest value of the ^{36}Cl/Cl ratio occurs at the LGM (N-4), which corresponds to a glacial period (low sea-level stand) with a larger ^{36}Cl/Cl ratio because of lowered Cl^{-} concentration in recharge. Based on the relatively low paleorecharge temperatures throughout the upper Patapsco aquifer, it is likely that most of the water sampled was recharged during past glacial periods, which

 DOI 10.1007/s10040-012-0871-1

argues for relatively high and constant values of the initial $^{36}Cl/Cl$ ratio.

^{36}Cl-calibrated radiogenic ^{4}He accumulation rates

The last column of Table 6 gives the value of the radiogenic ^{4}He accumulation rate needed to match the ^{36}Cl age. The radiogenic ^{4}He accumulation rates derived from the ^{36}Cl data vary from 1.24 to 3.46×10^{-12} $cm^3STP\ g^{-1}\ a^{-1}$, and are similar to the range of values derived from the U-Th calculation and the calibration to ^{14}C ages (Table 7). Excluding sample S-10, the average ^{36}Cl-calibrated ^{4}He accumulation rate for the upper Patapsco is $(2.2\pm0.9)\times10^{-12}$ $cm^3STP\ g^{-1}\ a^{-1}$, which compares to the average value of $(2.8\pm1.8)\times10^{-12}$ $cm^3STP\ g^{-1}\ a^{-1}$ calculated in the preceding from the U and Th analyses in the upper Patapsco sediment. It appears then that the ^{36}Cl ages of the low-Cl^- samples are consistent with values of the radiogenic ^{4}He accumulation rates within the upper Patapsco aquifer.

Spatial variations in ^{4}He accumulation rate

As a further refinement to the application of ^{4}He accumulation rates, the northern and southern flow path samples were treated separately. Radiogenic ^{4}He accumulation rates derived separately for the northern and southern flow paths are compared in Fig. 12. There is one outlier in the U-Th ^{4}He accumulation rates for samples from core KE Bf 149 on the southern flow path which is 4 times larger than the rate for the adjacent core (CH Bf 144) (Table 8); the value from KE Bf 149 was not included in the averaging, but included in Fig. 12 and Table 8. The average ^{36}Cl-calibrated ^{4}He accumulation rate (Table 8) is higher on the northern flow path ($(2.7\pm1.1)\times10^{-12}$ $cm^3STP\ g^{-1}\ a^{-1}$) than on the southern flow path ($(1.7\pm0.9)\times10^{-12}$ $cm^3STP\ g^{-1}\ a^{-1}$. Separating the six upper Patapsco cores sampled (Fig. 1) between the northern flow path (KE Bf 180, KE Cb 103, and QA Ef 29) and southern flow path (CH Bf 144, CH Bf 149, SM Df 84), the average U-Th-calculated ^{4}He accumulation rate is $(3.4\pm2.0)\times10^{-12}$ $cm^3STP\ g^{-1}\ a^{-1}$ for 17 upper Patapsco samples along the northern flow path and $(1.4\pm1.3)\times10^{-12}$ $cm^3STP\ g^{-1}\ a^{-1}$ for 7 samples along the southern flow path (Fig. 12, Table 8). The average ^{14}C-calibrated ^{4}He accumulation rate also is higher on the northern flow path, $(3.6\pm0.3)\times10^{-12}$ $cm^3STP\ g^{-1}\ a^{-1}$, than the one rate obtained for the southern flow path, 2.5×10^{-12} $cm^3STP\ g^{-1}\ a^{-1}$ (Fig. 12, Table 8). These differences indicate a rather wide range of heterogeneity in U and Th content in the upper Patapsco Formation which may be typical of the complex fluvial/deltaic depositional environment. Still, the data of Table 8 indicate higher U-Th radiogenic ^{4}He accumulation rates on the northern flow path than on the southern flow path and are in good agreement with the ^{36}Cl-calibrated and ^{14}C-calibrated ^{4}He accumulation rates (Fig. 12; Table 8).

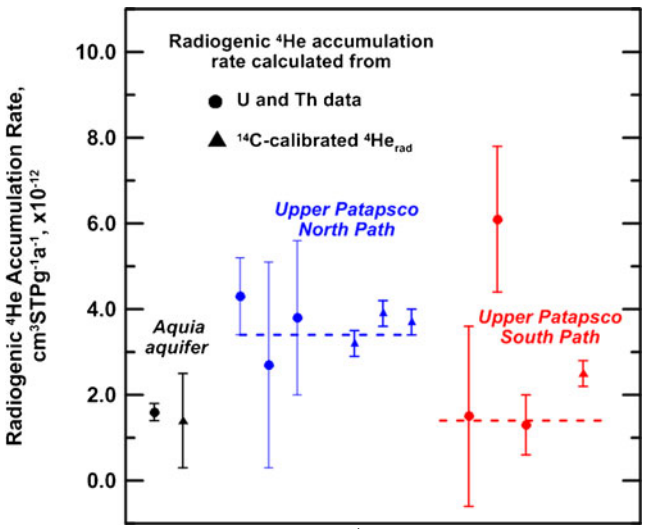

Fig. 12 Comparison of radiogenic ^{4}He accumulation rates for the Aquia aquifer (*black*, data of Aeschbach-Hertig 2002), with values from the northern (*blue*) and southern (*red*) flow paths of the upper Patapsco aquifer (this study) calculated either from U-Th data (*solid circles*) or ^{14}C-calibrated radiogenic ^{4}He data. *Dashed lines* show average U-Th radiogenic ^{4}He accumulation rates for north and south paths. The high value on the southern flow path is anomalous and was not included in the average

From their measurements of U and Th in Aquia sediment samples, Aeschbach-Hertig et al. (2002) calculated a radiogenic ^{4}He accumulation rate of $(1.6\pm0.2)\times10^{-12}$ $cm^3STP\ g^{-1}\ a^{-1}$, which is similar to that found for the southern flow path in the upper Patapsco. Most of the Aquia water samples had radiogenic ^{4}He ages of less than 80 ka, extending into the last glacial period (LGP) preceding the LGM. One sample (MD4, chloride content of 1.91 mg L^{-1}) at the farthest point sampled downgradient in the Aquia had an apparent ^{4}He age of about 280 ka.

The radiogenic ^{4}He accumulation ages in the upper Patapsco were calculated on the northern and southern flow paths using (1) the average U-Th ^{4}He accumulation rates for the northern and southern flow paths (Table 8) and (2) the average ^{36}Cl-calibrated ^{4}He accumulation rates for the northern and southern flow paths, in conjunction with the measured radiogenic ^{4}He concentrations at all northern and southern flow path wells, respectively (Table 9). The ^{4}He and ^{36}Cl-calibrated ^{4}He ages are plotted in Fig. 13 as a function of flow distance from the recharge zone.

Paleo-hydrogeologic implications

There are relatively few aquifers in which groundwater ages approaching the million-year timescale have been demonstrated (see for example, Phillips et al. 1986; Collon et al. 2000; Lehmann et al. 2003; Sturchio et al. 2004), and none have previously been recognized in the Atlantic Coastal Plain aquifers. This study reports ages of 500 ka to possibly the million-year timescale in parts of the upper Patapsco aquifer of Maryland, and therefore, the samples investigated here represent recharge from parts of as many as the last five to ten glacial cycles (Lisiecki and

 DOI 10.1007/s10040-012-0871-1

Table 8 Average calculated U-Th ^{4}He accumulation rates in upper Patapsco Formation[a]

Path	Core	U 238 μg g^{-1}	Th 232 μg g^{-1}	No. samples[b]	Average U-Th ^{4}He accumulation rate cm^{3}STP g^{-1}	No. samples	Average ^{14}C-calibrated ^{4}He accumulation rate ccSTP g^{-1}year^{-1}	No. samples	Average ^{36}Cl-calibrated ^{4}He accumulation rate ccSTP g^{-1} a^{-1}
North	KECb 103	3.0±0.4	11.3±3.3	4	$(4.3\pm0.9)\times10^{-12}$				
North	KEBf 180	1.6±1.6	8.2±7.4	8	$(2.7\pm2.4)\times10^{-12}$				
North	QAEd 29	2.8±1.2	9.3±4.6	5	$(3.8\pm1.8)\times10^{-12}$				
Avg.				17	$(3.4\pm2.0)\times10^{-12}$	4	$(3.6\pm0.3)\times10^{-12}$	3	$(2.7\pm1.1)\times10^{-12}$
South	CHBf 144	0.9±1.4	4.1±5.3	3	$(1.5\pm2.1)\times10^{-12}$				
South	KEBf 149	5.6±4.0	10.4±7.0	3	$(6.1\pm1.7)\times10^{-12}$				
South	SMDf 84	1.0±0.4	3.1±2.1	4	$(1.3\pm0.7)\times10^{-12}$				
Avg.				7[c]	$(1.4\pm1.3)\times10^{-12}$	1	2.5×10^{-12}	3	$(1.7\pm0.9)\times10^{-12}$

[a] See Fig. 1 for core locations. All samples from upper Patapsco; confining layers and clay-rich samples excluded

[b] Includes replicates

[c] Excludes core KEBf 149

Raymo 2005; Lüthi et al. 2008). Although multiple glacial cycles likely recharged waters older than about 20 ka in the upper Patapsco aquifer, only the LGM was clearly delineated.

Age increases with flow distance (Figs. 10, 11 and 13), in a non-linear fashion that indicates flow rates consistently decrease downgradient in the upper Patapsco aquifer. This may result from an aquifer system in which flow first moves laterally through the aquifer but later moves upward through confining layers to discharge to surface water or land surface. In the upper Patapsco, as in many coastal margin sedimentary aquifers, a saltwater interface provides a seaward barrier to freshwater flow, forcing horizontal velocity to zero at the interface. The inverse slope of a curve fit to data in Fig. 13 such as the empirical fit shown, gives linear velocity (Darcy velocity/porosity). The linear velocity is 1.0 m a^{-1} at a distance of 10 km upgradient of the LGM and downgradient of the LGM velocity decreases from 0.13 m a^{-1} at a distance of 40 km to 0.04 m a^{-1} at distance of 80 km.

Other factors also may contribute to the age pattern of Fig. 13. Upward leakage of old water from the lower

Table 9 Summary of path-specific ^{4}He accumulation ages

Site no.	^{4}He age from U-Th radiogenic ^{4}He accumulation rate $(3.4\pm2.0)\times10^{-12}$ cm^{3}STP g^{-1} a^{-1} (north) and $(1.4\pm1.3)\times10^{-12}$ cm^{3}STP g^{-1} a^{-1} (south)		^{4}He age from ^{36}Cl-calibrated radiogenic ^{4}He accumulation rate $(2.7\pm1.1)\times10^{-12}$ cm^{3}STP g^{-1} a^{-1} (north) and $(1.7\pm0.9)\times10^{-12}$ cm^{3}STP g^{-1} a^{-1} (south)		^{4}He age from ^{14}C-calibrated radiogenic ^{4}He accumulation rate $(3.6\pm0.3)\times10^{-12}$ cm^{3}STP g^{-1} a^{-1} (north) and $(2.5\pm0.3)\times10^{-12}$ cm^{3}STP g^{-1} a^{-1} (south)[c]	
	Age, ka	Age range, ka	Age, ka	Age range, ka	Age, ka	Age range, ka
N-1	ND	ND	ND	ND	ND	ND
N-2	13	8–32	17	12–28	13	12–14
N-3	18	11–44	23	16–38	17	16–19
N-4	24	15–58	30	21–51	22	21–25
N-4[a]	24	15–57	30	21–50	22	21–24
N-5	143	90–347	180	128–304	135	125–147
N-5[a]	142	90–346	179	127–303	135	124–147
N-6	297	187–722	374	266–632	281	259–306
N-6[a]	298	188–725	376	267–634	282	260–307
S-1	31	16–433	25	11–27	12	11–13
S-2	165	86–2,310	136	61–144	64	59–70
S-2[a]	164	85–2,298	135	60–144	64	59–70
S-3	340	176–4,764	280	125–298	132	122–144
S-4	450	233–6,303	371	166–394	175	162–191
S-4[a]	443	230–6,202	365	163–388	172	159–188
S-5	487	252–6,817	401	179–426	189	175–207
S-5[b]	488	253–6,831	402	180–427	190	175–207
S-6	496	257–6,948	409	183–434	193	178–211
S-7	648	336–9,074	534	239–567	252	233–275
S-8	650	337–9,107	536	240–569	253	234–276
S-8[b]	656	340–9,179	540	242–574	255	235–278
S-9	798	414–11,176	657	294–698	310	287–339
S-9[a]	791	410–11,074	651	291–692	308	308–336
S-10	6,005	3,114–84,068	4,945	2,212–5,254	2,335	2,156–2,548
S-10[a]	6,104	3,165–85,451	5,027	2,249–5,341	2,374	2,191–2,589

[a] Re-sampled for ^{36}Cl analysis

[b] Replicate analysis, QA/QC

[c] Uncertainty in ^{4}He accumulation rate for southern path assumed that of the northern path

 DOI 10.1007/s10040-012-0871-1

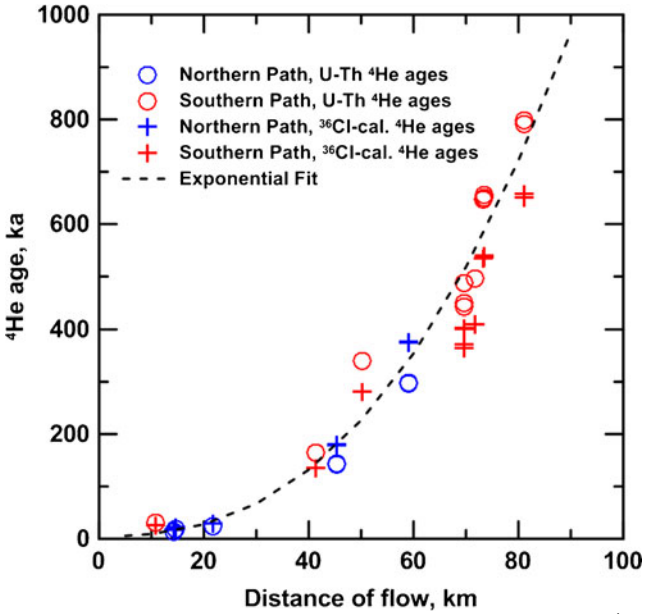

Fig. 13 Comparison of flow-path-specific U-Th radiogenic ^{4}He ages and ^{36}Cl-calibrated radiogenic ^{4}He ages calculated as a function of distance of flow from the recharge zone. The ages increase in a non-linear fashion with distance of flow on the northern and southern flow paths. The inverse slope of the empirical exponential curve fit ($y=AX^{a}+BX+C$, where y is age in ka, X is distance of flow in km, and A, a, B, and C are fitted empirical constants equal to 0.0125, 2.5, 0.01 and 5.0, respectively) gives a linear velocity of about 1.0 m a^{-1} at a distance of 10 km upgradient of the LGM. Downgradient of the LGM the velocity decreases with flow distance from 0.13 m a^{-1} at 40 km to 0.04 m a^{-1} at 80 km of flow. The pattern in groundwater flow velocities is consistent with the recharge hypothesis suggested for the Aquia aquifer by Purdy et al. (1996)

Patapsco (and below) may mix with the upper Patapsco waters, and leakage of old water from confining layers could contribute to increase in apparent age with flow distance, particularly with regard to sample S-10. Furthermore, the observations of Fig. 13 should be tempered by the fact that all of the water samples of this study were taken from production wells that, because they were constructed to produce maximum amounts of water, were screened in the more conductive zones in the upper Patapsco. This could lead to a young bias in interpreted age relative to water in low conductivity zones. Although the details of the flow field depend on the hydrogeologic structure of the aquifer and spatial distribution of hydraulic characteristics, the overall picture is of velocity decreasing with flow distance (Fig. 13).

The results for the upper Patapsco aquifer are consistent with findings for the Aquia aquifer of Purdy et al. (1996) who proposed that during glacial periods (low sea-level stands), the Aquia aquifer was flushed more rapidly due to increased hydraulic-head gradients in the upgradient part of the aquifer, than during interglacial periods (high sea-level stands). The estimated flow velocities for parts of the Aquia aquifer downgradient of the LGM were 0.2 m a^{-1} and yielded ages of more than 100 ka, based on hydraulic evidence (Purdy et al. 1996). Apparently then, the flow velocities in downgradient parts of the more shallow Aquia aquifer are some 2- to 5-fold greater than those in downgradient parts of the upper Patapsco aquifer. Aeschbach-Hertig et al. (2002) showed that the Cl^{-} minimum in Aquia aquifer water also corresponds to a minimum in NGRTs, supporting the interpretation of Purdy et al. (1987, 1992, 1996) that the Cl^{-} minimum represents recharge from the LGM and low sea-level stand.

The lowest NGRT from the Aquia aquifer attributed to the LGM was obtained from sample MD18, which was analyzed in duplicate, and averaged 3.3±0.3 °C (Aeschbach-Hertig et al. 2002). In the upper Patapsco aquifer, the LGM is near site N-4 which was sampled on two separate dates (this study) yielding an average NGRT of 1.4±1.0 °C (Table 5). The measured N_2–Ar recharge temperatures (Table 3) support the NGRTs of this study. If the modern mean annual recharge temperature is taken as 13 °C (this study), a maximum cooling at the LGM of about 10 °C relative to the Holocene is found for the Aquia NGRTs, which compares to an apparent maximum cooling of about 12 °C in recharge at the LGM in the upper Patapsco aquifer. This difference in NGRTs between the Aquia and upper Patapsco at the LGM is small, and may be within the propagated uncertainty in NGRTs for both studies. Other factors possibly contributing to this difference include failure to sample groundwater recharged at the same time in different aquifers, and differences in recharge conditions for the two aquifers. Considering the location of sample sites, the Aquia samples would have been recharged by infiltration through the unsaturated zone of the Aquia outcrop area, while samples from the northern flow path in the upper Patapsco would have been recharged, at least in part, by infiltration from the ancestral Susquehanna River at the LGM.

Both the northern and southern flow paths in the upper Patapsco appear to have been recharged in part by river water during the LGM. The very low recharge temperatures and depleted stable isotope signature at the LGM on the northern flow path (at N-4) suggests seepage from the ancestral Susquehanna River in areas where the paleo river channel crossed the outcrop zone of the upper Patapsco (Colman et al. 1990). The northern flow path waters are more depleted in stable isotope composition and have lower paleorecharge temperatures than those of the southern flow path, presumably because they contain fractions of glacial melt water derived from glacial outwash within the Susquehanna River drainage basin. The southern flow path appears to have been recharged during glacial periods by infiltration from the more southwesterly sourced ancestral Potomac River where the river channel and flood plains cross the outcrop of the upper Patapsco (Fig. 1). The southern flow path waters have lower D_{excess} than those of the northern flow path, possibly reflecting a moisture source at somewhat higher relative humidity than that of the northern flow path. Recharge through the flood plains and river valley of the southwesterly sourced ancestral Potomac River may explain why waters from the southern flow path have warmer recharge temperatures than the northern flow path

 DOI 10.1007/s10040-012-0871-1

(Fig. 8) (the later containing relatively high fractions of glacial melt water recharge from the ancestral Susquehanna River). Finally, the higher amounts of excess air in the southern flow path waters relative to those of the northern flow path are consistent with trapping of air from ponded recharge as opposed to direct infiltration from the channel of the ancestral Susquehanna River.

Only the first sample on the northern flow path contains modern water. All other samples have relatively low recharge temperatures that suggest the upper Patapsco aquifer was recharged primarily during glacial periods (low sea-level stands). The samples located within the first 60 km of flow downgradient have ages that cluster around 10–20 ka, 150 ka, and approximately 270–300 ka (Fig. 13), which corresponds to the approximate timeframes of past glacial periods (see for example, Crowley and North 1991). These ages also are similar to the approximate ages of the past three generations of the ancestral Susquehanna River System beneath Chesapeake Bay (Colman et al. 1990).

Tracer patterns delineating glacial cycles earlier than the LGM in the upper Patapsco may be lost to dispersive mixing in the aquifer, to mixing during pumping across multiple screened intervals of aquifer, or, in most cases, were not even sampled due to spatial location of wells. Another factor is that the Coastal Plain aquifers are recharged predominantly during glacial periods when sea level and coastal heads are lowered, and hydraulic gradients are steeper between recharge and discharge. Therefore it would be unlikely to detect either the brief glacial maxima or relatively brief interglacial periods. What remains is recharge from the relatively long glacial periods.

Future hydrologic investigations should be expanded to areas south of the study area and focus on the possible role that low-permeability sediment associated with the Chesapeake Bay impact crater (Powars and Bruce 1999; Sanford et al. 2009), located at the mouth of Chesapeake Bay, influence groundwater movement and hence groundwater age. In addition, better estimates of aquifer hydraulic properties (porosity) and groundwater flow rates and directions from regional flow analysis throughout the Mid-Atlantic region are needed.

Implications for groundwater management

The results of this study demonstrate that groundwater pumped from most parts of the upper Patapsco aquifer of Maryland is non-renewable on human timescales under natural gradients. Large depressions in hydraulic head have developed in the upper Patapsco aquifer, as well as several other aquifers of the Atlantic Coastal Plain of Maryland (Shedlock et al. 2007; Drummond 2007; Soeder et al. 2007). Groundwater-flow modeling studies of the confined aquifers in the Maryland Atlantic Coastal Plain indicate that recharge increases from the outcrop part of the aquifers in response to groundwater withdrawals, both as infiltration at the land surface and leakage from the Potomac River (Andreasen 2007; Drummond 2007). As a result, the induced recharge could balance the increased withdrawals and maintain the equilibrium of the aquifer system. Because most of the water in the upper Patapsco aquifer is very old, it is especially critical for the sustainable utilization of the resource, that the balance between recharge and withdrawals be managed carefully. Future research into aquifer-system budget dynamics (flow modeling) should be conducted to support water-management decisions. The groundwater ages interpreted here will aid in refinement of future groundwater models developed to manage the resource. In addition, alternative management strategies such as aquifer storage and recovery may have to be considered to help achieve sustainability.

Summary and conclusions

As a part of a study to develop management tools to aid in sustainable utilization of the groundwater resources of the Maryland Atlantic Coastal Plain, apparent groundwater ages in parts of the upper Patapsco aquifer of the Maryland Atlantic Coastal Plain were estimated along two generalized flow paths (Fig. 1), using a suite of naturally occurring environmental tracers. Helium-4 accumulation ages were calculated from the measured amounts of radiogenic ^{4}He in upper Patapsco groundwater using three separate estimates of the ^{4}He accumulation rates: (1) those calculated from measurements of U and Th in samples from upper Patapsco core, (2) those calculated from ^{14}C-calibrated radiogenic ^{4}He accumulation rates, and (3) those calculated from ^{36}Cl-calibrated ^{4}He accumulation rates. The derived average radiogenic ^{4}He accumulation rates are (1) $(2.8\pm1.8)\times10^{-12}$ $cm^3STP\ g^{-1}\ a^{-1}$, (2) $(3.4\pm0.6)\times10^{-12}$ $cm^3STP\ g^{-1}\ a^{-1}$, and (3) $(2.2\pm0.9)\times10^{-12}$ $cm^3STP\ g^{-1}\ a^{-1}$, respectively. The radiogenic ^{4}He accumulation rates derived from the ^{36}Cl data vary from 1.24 to 3.46×10^{-12} $cm^3STP\ g^{-1}\ a^{-1}$, and are similar to the range of values derived from the U-Th calculation and the calibration to ^{14}C ages. This indicates that the ^{14}C, ^{36}Cl and U-Th ^{4}He ages are consistent, generally within a factor of 2 or better. Age estimates were refined further by accounting for regional variations in U and Th content of the upper Patapsco Formation, demonstrating somewhat higher ^{4}He accumulation rates on the northern flow path relative to those on the southern flow path (Table 9). Final age estimates were calculated using flow path-specific U-Th radiogenic ^{4}He accumulation rates $(3.4\pm2.0)\times10^{-12}$ $cm^3STP\ g^{-1}\ a^{-1}$ (northern flow path) and $(1.4\pm1.3)\times10^{-12}$ $cm^3STP\ g^{-1}\ a^{-1}$ (southern flow path), and flow path-specific ^{36}Cl-calibrated ^{4}He accumulation rates $(2.7\pm1.1)\times10^{-12}$ $cm^3STP\ g^{-1}\ a^{-1}$ (northern flow path) and $(1.7\pm0.9)\times10^{-12}$ $cm^3STP\ g^{-1}\ a^{-1}$ (southern flow path; Table 9).

The LGM was located approximately 20 km downgradient along the northern flow path (at site N-4) where the dissolved gas paleorecharge temperatures were 0.5–1.5 °C, and dissolved Cl^-, Cl/Br and $\delta^{18}O$ were minimum. The adjusted ^{14}C age at N-4 was 21.5 ka. The LGM

 DOI 10.1007/s10040-012-0871-1

occurs in the Aquia aquifer, located above the upper Patapsco (Fig. 2) at a flow distance of 40 km (Aeschbach-Hertig et al. 2002). This difference indicates that average flow velocities in upgradient parts of the Aquia aquifer are about two-fold greater than those of upgradient parts of the upper Patapsco aquifer, 2 m a^{-1} compared to 1.0 m a^{-1}, respectively. Flow velocities decrease with increasing distance of flow, perhaps due to mass-balance considerations of aquifer leakage upward to surface discharge. Flow velocities downgradient from the LGM ranged from about 0.04–0.13 m a^{-1}, which is 2–5 fold slower than the average flow velocity of 0.2 m a^{-1} reported by Purdy et al. (1996) for downgradient parts of the Aquia aquifer.

Apparent ages in the upper Patapsco aquifer range from 0 to 50 ka in the upgradient part of the flow system, but are considerably older downgradient, indicating that the upgradient parts were flushed relatively rapidly during glacial periods, as originally proposed by Purdy et al. (1996). The dissolved gas recharge temperatures typically are in the range of 5–7 °C, some 6–8 °C lower than today in the upper Patapsco, indicating that recharge was predominantly during glacial periods, when coastal heads were lowered due to low sea-level stands. The deeper parts of the upper Patapsco aquifer seem to discharge more slowly, probably because they are under numerous confining layers, and bounded horizontally by a saltwater interface (Fig. 2). The upgradient parts of these aquifers can discharge more rapidly by upward leakage through more shallow confining layers, can discharge to more shallow aquifers, and to surface drainage along the western edge of Chesapeake Bay. The older waters in the upper Patapsco (500 ka) appear to be considerably older than that suggested for the Aquia. The oldest water at the end of the southern flow path (at S-10) appears to be at or near secular equilibrium with ^{36}Cl, and has an average U-Th radiogenic ^{4}He accumulation age of about 2.5–3.0 Ma.

The upper Patapsco of Maryland is recharged along the northern flow path by infiltration of meteoric water and probably by seepage from the ancestral Susquehanna River in areas where the paleo river channel would have crossed the outcrop zone of the upper Patapsco during glacial periods. Along the southern flow path recharge is at least in part from the Potomac River, because the flood plains of the Potomac River valley cross the outcrop of the upper Patapsco. Most of the waters along the southern flow path have lower D_{excess} than those of the northern flow path, and may contain waters derived from the Potomac River drainage basin sourced to the southwest of the study area. Infiltration from the ancestral Susquehanna River during glacial periods may account for depleted stable isotope composition along the northern flow path relative to that of the southern flow path.

Most parts of the Atlantic Coastal Plain of Maryland rely on groundwater as the primary source of freshwater supply, and increasingly, water managers are turning to the deeper aquifers, such as the upper Patapsco aquifer. This study demonstrates that most water in the upper Patapsco is non-renewable on human timescales under natural gradients, thus highlighting the importance of effective water-supply management to prolong the resource.

Acknowledgements This study was conducted by the US Geological Survey (USGS) in cooperation with the Maryland Geological Survey (MGS) and Maryland Department of the Environment (MDE). Chemical analyses of water and rock samples were provided by Michael Doughten, USGS, Reston VA. David Drummond (MGS, Baltimore, MD) assisted in locating upper Patapsco core from the study area. Daniel Webster (USGS, Reston, VA) provided core sampling, x-ray diffraction analysis, and rock sample preparation, and Sarah Ingle (USGS, Reston, VA) assisted in processing rock samples for analysis. Peggy Widman (USGS, Reston, VA) provided gas chromatographic analyses of N_2 and Ar in water samples and Julian Wayland (USGS, Reston, VA) assisted in field sampling and chlorofluorocarbon analyses. Robert Michel (USGS, Menlo Park, CA) provided tritium analyses, and Tyler Coplen (USGS, Reston, VA) provided the stable isotope analyses. Drafting assistance was provided by Tim Auer (USGS, Baltimore, MD). The ^{36}Cl and ^{14}C measurements were made at PRIME Lab (Purdue University) and the NOSAMS facility (Woods Hole, MA), respectively. The manuscript was improved by the constructive reviews of Ate Visser (LLNL, Livermore, CA), Richard M. Yager (USGS, Ithaca, NY), and three anonymous reviewers. Any use of trade, firm, or product names is for descriptive purposes only and does not imply endorsement by the US Government.

References

Aeschbach-Hertig W, Peeters F, Beyerle U, Kipfer R (1999) Interpretation of dissolved atmospheric noble gases in natural waters. Water Resour Res 35:2779–2792

Aeschbach-Hertig W, Peeters F, Beyerle U, Kipfer R (2000) Paleotemperature reconstruction from noble gases in ground water taking into account equilibration with entrapped air. Nature 405:1040–1044

Aeschbach-Hertig W, Stute M, Clark JF, Reuter RF, Schlosser P (2002) A paleotemperature record derived from dissolved noble gases in groundwater of the Aquia Aquifer (Maryland, USA). Geochim Cosmochim Acta 66(5):797–817

Andreasen DC (2007) Optimization of ground-water withdrawals in Anne Arundel County, Maryland, from the Upper Patapsco, Lower Patapsco, and Patuxent aquifers projected through 2044. Maryland Geol Surv Rep Invest 77, MGS, Baltimore, MD

Andreasen DC, Achmad G, Staley AW, Hodo RM (2007) Hydrogeologic framework of the Maryland Coastal Plain. Maryland Geol Surv Prog Rep, MGS, Baltimore, MD

Andrews JN, Lee DJ (1979) Inert gases in groundwater from the Bunter Sandstone of England as indicators of age and palaeoclimatic trends. J Hydrol 41:233–252

Balderer W, Synal H-A (1996) Application of the chlorine-36 method for the characterization of the groundwater circulation in tectonically active areas: examples from northwestern Anatolia/Turkey. Terra Nova 8(4):324–333. doi:10.1111/j.1365-3121.1996.tb00565.x

Bayer R, Schlosser P, Banisch G, Rupp H, Zaucker F, Zimmek G (1989) Performance and blank components of a mass spectrometic system for routine measurement of helium isotopes and tritium by ^{3}He ingrowth method. In: Sitzungsberichte der Heidelberger Akademie der Wissenschaften. Mathematisch-naturwissenschaftliche Klasse, Springer, Heidelberg, pp 241–279

Bentley HW, Phillips FM, Davis SN (1986) Chlorine-36 in the terrestrial environment. In: Fritz P, Fontes J-C (eds) Handbook of environmental isotope geochemistry, vol 2. Elsevier, Amsterdam

Beyerle U, Aeschbach-Hertig W, Imboden DM, Baur H, Graph T, Kipfer R (2000) A mass spectrometric system for the analysis of noble gases and tritium from water samples. Environ Sci Technol 34(10):2042–2050

 DOI 10.1007/s10040-012-0871-1

Bintanja R, van de Wal RS, Oerlemans J (2005) Modelled atmospheric temperatures and global sea levels over the past million years. Nature 437:126–128

Busenberg E, Plummer LN (1992) Use of chlorofluorocarbons (CCl_3F and CCl_2F_2) as hydrologic tracers and age-dating tools: example—the alluvium and terrace system of central Oklahoma. Water Resour Res 28(9):2257–2284

Collon P, Kutschera W, Loosli HH, Lehmann B, Purtschert R, Love A, Sampson L, Anthony D, Davids B, Cole D, Morrissey D, Pardo R, Paul M, Sherrill B, Steiner M (2000) ^{81}Kr in the Great Artesian Basin, Australia: a new method for dating very old groundwater. Earth Planet Sci Lett 182:103–113

Colman SM, Halka JP, Hobbs CH III, Mixon RB, Foster DS (1990) Ancient channels of the Susquehanna River beneath Chesapeake Bay and the Delmarva Peninsula. Geol Soc Am Bull 102:1268–1279

Coplen TB (1994) Reporting of stable hydrogen, carbon, and oxygen isotopic abundances. Pure Appl Chem 66:273–276

Coplen TB, Kendall C (2000) Stable hydrogen and oxygen isotope ratios for selected sites of the US Geological Survey's NASQAN and Benchmark surface-water networks. US Geol Surv Open-File Rep 00-160, 97 pp

Crowley TJ, North GR (1991) Paleoclimatology. Oxford Univ Press, New York

Davis SN, DeWayne C, Zreda M, Sharma P (1998) Chlorine-36 and the initial value problem. Hydrogeol J 6:104–114

Davis SN, Fabryka-Martin J, Wolfsberg L, Moysey S (2000) Chlorine-36 in ground water containing low chloride concentrations. Ground Water 38:912–922

Davis SN, Moysey S, Cecil LD, Zreda M (2003) Chlorine-36 in groundwater of the United States: empirical data. Hydrogeol J 11:217–227

Davis SN, Fabryka-Martin JT, Wolfsberg LE (2004) Variations in bromide in potable ground water in the United States. Ground Water 42:902–909

Drummond DD (2007) Water-supply potential of the Coastal Plain aquifers of Calvert, Charles, and St. Mary's Counties, Maryland, with emphasis on the upper Patapsco and lower Patapsco aquifers. Rep Invest 76, Depart Nat Resour, Resour Assess Serv, Maryland Geological Survey, Baltimore, MD, 225 pp

Duigon MT, Bolton DW (2003) Formation geochemistry at two boreholes and its bearing on radium content of ground water, Anne Arundel County, Maryland. Maryland Geol Surv Open-File Rep 2003-02-15, MGS, Baltimore, MD

Elmore D, Phillips FM (1987) Accelerator mass spectrometry for measurement of long-lived radioisotopes. Science 236:543–550

Fleck WB, Andreasen DC (1996) Geohydrologic framework, ground-water quality and flow, and brackish-water intrusion in east-central Anne Arundel County, Maryland, with a section on Simulation of brackish-water intrusion in the Aquia aquifer in the Annapolis area using a solute-transport model, by Barry S. Smith. Maryland Geol Surv Rep Invest 62, MGS, Baltimore, MD, 136 pp

Fontes JCh, Garnier JM (1979) Determination of the initial activity of the total dissolved carbon: a review of existing models and a new approach. Water Resour Res 12:399–413

Gleeson T, VanderSteen J, Sophocleous MA, Taniguchi M, Alley WM, Allen DM, Zhou Y (2010) Groundwater sustainability strategies. Nature Geosci 3:378–379

Hansen HJ (1969) Depositional environments of the subsurface Potomac Group in southern Maryland. Am Assoc Pet Geol Bull 53(9):1923–1937

Hansen HJ (1977) Geologic and hydrologic data from two core holes drilled through the Aquia formation (eocene-paleocene), in Prince George's and Queen Anne's counties, Maryland. Maryland Geol Surv Open File Rep 77-02-1, MGS, Baltimore, MD

Hansen HJ, Wilson JM (1984) Summary of hydrogeologic data from a deep (2,678ft.) well at Lexington Park, St. Mary's county, Maryland. Maryland Geol Surv Open File Rep 84-02-1, MGS, Baltimore, MD

Katz BG, Eberts SM, Kauffman LJ (2011) Using Cl/Br ratios and other indicators to assess potential impacts on groundwater quality from septic systems: a review and examples from principal aquifers in the United States. J Hydrol 398:151–166

Kendall C, Coplen TB (2001) Distribution of Oxygen-18 and Deuterium in river waters across the United States. Hydrol Process 15:1363–1393. doi:10.1002/hyp.217

Koterba MT, Wilde FD, Lapham WW (1995) Ground-water data-collection protocols and procedures for the National Water-Quality Assessment Program: collection and documentation of water-quality samples and related data. US Geol Surv Open-File Rep 95-399, 113 pp

Lehmann BE, Love A, Purtschert R, Collon P, Loosli HH, Kutschera W, Beyerle U, Aeschbach-Hertig W, Kipfer R, Frape SK, Herczeg A, Moran J, Tolstikhin IN, Gröning M (2003) A comparison of groundwater dating with ^{81}Kr, ^{36}Cl and ^{4}He in four wells of the Great Artesian Basin, Australia. Earth Planet Sci Lett 211:237–250

Lisiecki LE, Raymo ME (2005) A Pliocene-Pleistocene stack of 57 globally distributed benthic $\delta^{18}O$ records. Paleoceanography 20: PA1003. doi:10.1029/2004PA001071

Lüthi D, Le Floch M, Bernhard B, Blunier T, Barnola J-M, Siegenthaler U, Raynaud D, Jouzel J, Fischer H, Kawamura K, Stocker TF (2008) High-resolution carbon dioxide concentration record 650,000-800,000years before present. Nature 453:379–382. doi:10.1038/nature06949

Masterson JP, Pope JP, Monti Jack Jr, Nardi MR (2011) Assessing groundwater availability in the Northern Atlantic Coastal Plain aquifer system. US Geol Surv Fact Sheet 2011–3019, 4 pp. Also available at http://pubs.usgs.gov/fs/2011/3019. Accessed 17 April, 2012

McFarland ER, Bruce TS (2006) The Virginia coastal plain hydrogeologic framework. US Geol Surv Prof Pap 1731, 119 pp. Available online at http://pubs.water.usgs.gov/pp1731/. Accessed 17 April, 2012

Merlivat L, Jouzel J (1983) Deuterium and ^{18}O in precipitation: a global model from oceans to ice caps. In: Palaeoclimates and paleowaters: a collection of environmental studies. STI/PUB/621, IAEA, Vienna, pp 65–66

Moysey S, Davis SN, Zrenda M (1999) A preliminary report on the distribution and variability of chlorine-36 in groundwater across the United States. Am Geophys Union Trans 80(17):S139, Abstract. Spring Meeting

Moysey S, Davis SN, Zreda M, Cecil LD (2003) The distribution of meteoric $^{36}Cl/Cl$ in the United States: a comparison of models. Hydrogeol J 11:615–627

Ozima M, Podosek FA (1983) Noble Gas Geochemistry. Cambridge University Press, Cambridge, 367 pp

Phillips FM (2000) Chlorine-36. In: Cook PG, Herczeg AL (eds) Environmental tracers in subsurface hydrology. Kluwer, Boston

Phillips FM, Bentley HW, Davis SN, Elmore D, Swanick GB (1986) Chlorine-36 dating of very old groundwater. 2. Milk River aquifer, Alberta, Canada. Water Resour Res 22:2003–2016

Plummer LN (1993) Stable isotope enrichment in paleowaters of the southeast Atlantic Coastal Plain, United States. Science 262:2016–2020

Plummer LN, Prestemon EC, Parkhurst DL (1994) An interactive code (NETPATH) for modeling NET geochemical reactions along a flow PATH: Version 2.0. US Geol Surv Water Resour Invest Rep 94-4169, 130 pp

Plummer LN, Bexfield LM, Anderholm SK, Sanford WE, Busenberg E (2004) Geochemical characterization of ground-water flow in the Santa Fe Group aquifer system, Middle Rio Grande Basin, New Mexico. US Geol Surv Water-Res Invest Rep 03-4131, 395 pp. http://pubs.usgs.gov/wri/wri034131/. Accessed 17 April 2012

Powars DS, Bruce TS (1999) The effects of the Chesapeake Bay impact crater on the geological framework and correlation of hydrogeologic units of the lower York-James Peninsula, Virginia. US Geol Surv Prof Pap 1612:82

Purdy CB, Mignerey AC, Helz GR, Drummond DD, Kubic PW, Elmore D, Hemmick T (1987) ^{36}Cl: a tracer in groundwater in the Aquia Formation of southern Maryland. Nucl Instrum Meth Phys Res B29:372–375

Purdy CB, Burr GS, Rubin M, Helz GR, Mignerey AC (1992) Dissolved organic and inorganic ^{14}C concentrations and ages for Coastal Plain aquifers in southern Maryland. Radiocarb 34 (3):654–663

Purdy CB, Helz GR, Mignerey AC (1996) Aquia aquifer dissolved Cl^- and $^{36}Cl/Cl$: Implications for flow velocities. Water Resour Res 32(5):1163–1171

Richards HG (1948) Studies of the subsurface geology and paleontology of the Atlantic Coastal Plain. Acad Nat Sci Proceed C 39–76

Sanford WE, Voytek MA, Powars DS, Jones BF, Cozzarelli IM, Cockell CS, Eganhouse RP (2009) Pore-water chemistry from the ICDP-USGS core hole in the Chesapeake Bay impact structure: implications for paleohydrology, microbial habitat, and water resources. In: Gohn GS, Koeberl C, Miller KG, and Reimold WU (eds) The ICDP-USGS Deep Drilling Project in the Chesapeake Bay Impact Structure: Results from the Eyreville Core Holes. Geol Soc Am Spec Pap 458:867–890

Shedlock RJ, Bolton DW, Cleaves ET, Gerhart JM, Nardi MR (2007) A science plan for a comprehensive regional assessment of the Atlantic Coastal Plain aquifer system in Maryland. US Geol Sur Open-File Rep 2007–1205, 25 pp

Soeder DK, Raffensperger JP, Nardi MR (2007) Effects of withdrawals on ground-water levels in southern Maryland and the adjacent Eastern Shore, 1980–2005. US Geol Surv Sci Invest Rep 2007–5249:82

Solomon DK, Hunt A, Poreda RJ (1996) Source of radiogenic helium 4 in shallow aquifers: implications for dating young groundwater. Water Resour Res 32:1805–1813

Sturchio NC, Du X, Purtschert R, Lehmann BE, Sultan M, Patterson LJ, Lu ZT, Müller P, Bigler T, Bailey K, OÇonnor TP, Young L, Lorenzo R, Becker R, Alfy ZE, Kaliouby BE, Dawood Y, Abdallah AMA (2004) One million year old groundwater in the Sahara revealed by krypton-81 and chlorine-36. Geophys Res Lett 31:L05503. doi:10.1029/2003GL019234

Stute M, Schlosser P (2000) Atmospheric noble gases. In: Cook PG, Herczeg AL (eds) Environmental tracers in subsurface hydrology. Kluwer, Boston, pp 349–377

Stute M, Sonntag C, Deak J, Schlosser P (1992) Helium in deep circulating groundwater in the Great Hungarian Plain: flow dynamics and crustal and mantle helium fluxes. Geochim Cosmochim Acta 56:2051–2067

Torgersen T, Clarke WB (1985) Helium accumulation in groundwater, I: an evaluation of sources and the continental flux of crustal ^4He in the Great Artesian Basin, Australia. Geochim Cosmochim Acta 49:1211–1218

US Geological Survey (2011a) Instructions for collecting stable isotope samples. US Geological Survey, Reston, VA. Available at http://isotopes.usgs.gov/lab/instructions.html. Accessed 17 April 2012

US Geological Survey (2011b) US Geological Survey, Reston Chlorofluorocarbon Laboratory. US Geological Survey, Reston, VA. Available at http://water.usgs.gov/lab/. Accessed 17 April 2012

US Geological Survey (2011c) US Geological Survey, Reston Chlorofluorocarbon Laboratory. US Geological Survey, Reston, VA. Available at http://water.usgs.gov/lab/dissolved-gas/lab/analytical_procedures/. Accessed on 17 April 2012

US Geological Survey (variously dated) National field manual for the collection of water-quality data. US Geological Survey Techniques of Water-Resources Investigations, book 9, chaps. A1–A9. Available at http://water.usgs.gov/owq/FieldManual/. Accessed 17 April 2012

Van der Straaten, CM, Mook, WG (1983) Stable isotopic composition of precipitation and climatic variability. In Palaeoclimates and Paleowaters: a collection of Environmental Studies. STI/PUB/621, IAEA, Vienna, 1983, pp 53-64

Woods Hole Oceanographic Institution (2011) NOSAMS, National Ocean Sciences Accelerator Mass Spectrometry Facility. The Sample Preparation Laboratory. Available at http://www.whoi.edu/page/live.do?pid=43315. Accessed on 17 April 2012